Abstract

DeBruhl, Christopher Dwayne. NO_x Formation in Unsteady Counterflow Diffusion Flames. (Under the direction of Dr. William L. Roberts)

The formation of NO and NO_2 are sensitive indicators of both temperature and residence time in a combustion environment. In this work, the NO_x emission index is measured in an unsteady counterflow diffusion flame with methane, propane or ethylene, as a function of average strain rate and amplitude and frequency an imposed sinusoidal oscillation. These flames varied from non-sooting to high soot loading, and from low average strain rate to near extinction. Due to the relatively long time scales associated with NO_x formation, the effect of unsteadiness on emission index is weaker than on either temperature or soot volume fraction. Time averaged global measurements were taken using a NO/NO_x analyzer. Methane – air results are compared with unsteady calculations using a modified OPPDIF code included in the Chemkin package.

NO_X FORMATION IN UNSTEADY COUNTERFLOW DIFFUSION FLAMES

By

Christopher Dwayne DeBruhl

A thesis submitted to the Graduate Faculty of
North Carolina State University
in partial fulfillment of the
requirements for the Degree of
Master of Science

AEROSPACE ENGINEERING

Raleigh

2003

APPROVED BY:

Dr. Fred R. DeJarnette Advisory Committee Member	Dr. Stefan Franzen Advisory Committee Member

Dr. William L. Roberts
Chair of Advisory Committee

Biography

Christopher Dwayne DeBruhl was born in Asheville, NC on January 29, 1978, and, after a brief period of moving around Western North Carolina, grew up in Mars Hill, NC. He lived with his parents Larry and Marsha DeBruhl and his sister Rachel DeBruhl. He attended Madison High School, where he enjoyed playing football, wrestling, running track, and playing lead trumpet in the wind ensemble and jazz bands. He graduated in May 1996, and enrolled at North Carolina State University. While at NCSU Dwayne earned his BS degree in aerospace engineering, and graduated in the spring of 2000. Dwayne then began working toward his master's degree, in the area of combustion research. Dwayne will begin his professional career as an aerospace engineer at Cherry Point Marine Corps Air Station, in Havelock, NC, working with helicopter gas turbine engines.

Acknowledgements

I would first like to thank my parents, Larry and Marsha, and sister, Rachel, for their unwavering love and support throughout my life. Without their support none of this would have been possible. They have always been there for me and I hope that I will be able to do the same. I would also like to thank my Love and best friend, Jeanette. I could not have made it through the last few years without her. Thank you for being you, and being in my life. Thank you to all the friends I have made at NCSU and, especially, in the MAE department. You've made my college experience unforgettable.

Thank you to Dr. William Roberts for the experience of working on this interesting project, and for always being there to answer questions and show support. Thank you to Dr. Tarek Echekki for the much needed support with the all of the computational work involved in this research. I would also like to acknowledge the support of Dr. David Mann from the Army Research Office. Partial support has for this research has been provided under grant DAAD19-00-1-0429.

Table of Contents

List of Figures

List of Tables

1 Introduction

NO_x, composed of NO, NO_2, and N_2O, is a pollutant formed by the combustion of fuel in air. In the lower atmosphere nitrogen dioxide (NO_2) is converted to nitric acid (HNO_3) which is a major contributor to acid rain. NO_x in the lower atmosphere is primarily produced by sources on the surface, such as automobiles and power generation facilities. Due to the nature of terrestrial combustion many methods can be incorporated to control NO_x emissions, primarily through control of the combustion process or after-gas treatment. Using pre-mixed flames allows for the control of the equivalence ratio, which has a direct effect on NO_x production through a reduction in the peak flame temperature.

Ozone (O_3) absorbs harmful ultra violet rays, keeping the flux of UV radiation which reaches the surface of the Earth, at a tolerable level. In the upper atmosphere nitric oxide (NO) is very aggressive in the destruction of ozone. This is a catalytic process because NO is regenerated, and a few molecules of NO can be responsible for the destruction of hundreds of O_3 molecules. It is difficult for NO_x produced on the surface to reach the upper atmosphere. The primary cause of NO_x in the stratosphere is high altitude aircraft such as commercial airliners. NO_x produced by these aircraft is particularly undesirable because it is inserted directly in the ozone layer.

Due to the nature of aeropropulsion, premixing the fuel and air is generally not feasible. Therefore, these engines use turbulent diffusion flames, which operate with a fixed equivalence ratio of unity. This means the combustion process operates at stoichmetric conditions and cannot be adjusted, which makes controlling NO_x emissions very difficult. Because these jet engines use turbulent diffusion flames in the combustion stage it is very important to understand how harmful emissions are formed in such flames.

The study of turbulent diffusion flames is very complicated because of its complicated multi-component flowfield, inherently unsteady nature, and the coupled interaction between the flowfield and chemical processes. For this reason combustion research has focused on simplifying the problem to one with simple chemistry (single step or reduced mechanisms) or full chemistry with a simple flow field. Neither of these approaches accurately models the chemistry in a real turbulent diffusion flame. Flamelet theory simplifies this analysis by treating the turbulent diffusion flame as an ensemble of strained, laminar, one-dimensional flamelets which can be described by one variable, the mixture fraction. The flamelet model can be extended to include the non-equilibrium effects of finite rate chemistry by introducing a new variable, the scalar dissipation rate, which is a function of the hydrodynamics of the flowfield. Flamelet theory will be discussed further in section 1.2.

Previous studies have shown that laminar counterflow diffusion flames under steady rates of strain exhibit many fundamental characteristics of flamelets (Spalding, 1961; Tsuji, 1982; Seshadri & Peters, 1988; Dixon & Lewis, 1984). Conversely, only few studies have looked at the response of counterflow diffusion flames to unsteady strain rates (Im et al., 1995; Sung et al., 1995; Egolfopoulos & Campbell, 1996; Im et al., 1998). Flamelet theory assumes the flamelets respond quasi-steadily to the instantaneous imposed strain field. Recent experimental and numerical results show this is not a good assumption for high frequency unsteadiness (Egolfopoulos, 2000; Welle et al., 2002).

This research involved experiments designed to study a flamelet's response to unsteady strain rates by taking time averaged measurements of the NO_x produced in a counterflow diffusion flame using an Analytical Instruments Model 400 HCLD NO/NO_x

analyzer. The flames studied vary from non-sooting to high soot loading, and from low average strain rate to near extinction. NO and NO_x measurements for both steady and unsteady flames are compared with calculations using a modified OPPDIF code, OPUS, included in the Chemkin package.

1.1 NO_x Formation

Many researchers have studied NO_x formation under many different conditions (Hayhurst & Vince, 1983; Miller & Bowman, 1989; Bowman, 1992). Many experimental studies have been done in premixed flames (Fenimore, 1971; Glarborg et al., 1986; Dupont & Williams, 1998; Charlston-Goch, 2001; Konnov et al., 2003) and in coflow and jet diffusion flames (Turns & Myhr, 1991; Turns, 1995; Smyth, 1996; Yamashita et al. 1997; Sanders et al., 1997; Caldeira-Pires et al., 2000; Frank et al., 2000; Beltarme et al., 2001; Dally et al., 2003). There have also been many studies in steady laminar counterflow diffusion flames which have yielded both experimental and computational data (Hahn & Wendt, 1981; Drake & Blint, 1989; Bonturi et al., 1996; Ravikrishna & Laurendeau, 1999; Lee et al., 2001; Fuse et al., 2002). Few researchers have focused on NO_x formation in unsteady flowfields. In general four production pathways are for NO_x are distinguishable. These include the thermal mechanism, prompt mechanism, NO production from fuel nitrogen, and the nitrogen dioxide mechanism.

1.1.1 Thermal NO mechanism

The thermal NO mechanism (or Zel'dovich mechanism) is comprised of the following chemical reactions,

$$N_2 + O \underset{k_2}{\overset{k_1}{\rightleftharpoons}} NO + N \tag{1.1}$$

$$N + O_2 \underset{k_4}{\overset{k_3}{\rightleftharpoons}} NO + O \tag{1.2}$$

$$N + OH \underset{k_6}{\overset{k_5}{\rightleftharpoons}} NO + H \tag{1.3}$$

$$O_2 + M \underset{k_8}{\overset{k_7}{\rightleftharpoons}} 2O + M \tag{1.4}$$

If the steady state assumption is applied to N atoms, and the concentration of NO is assumed to be small compared to the other concentrations, and if destructive reactions are neglected compared to the formation reactions, it can be shown that,

$$\frac{d[NO]}{dt} = 2k_1[O][N_2] \tag{1.5}$$

Applying the partial equilibrium assumption to reaction 1.4 the O atom concentration can be written as,

$$[O] = [O_2]_{eq}^{1/2} k_p (T)^{1/2} (R_u T)^{-1/2} \tag{1.6}$$

Combining these two assumptions yields,

$$\frac{d[NO]}{dt} = 2k_1 k_p (T)^{1/2} (R_u T)^{-1/2} [O_2]_{eq}^{1/2} [N_2]_{eq} \tag{1.7}$$

This equation shows the strong temperature dependence, because the k_i's are exponential in temperature, and somewhat weaker dependence on the O_2 concentration of the burned gas $[O_2]_{eq}$, on the NO formation rate.

Reactions 1.1-1.4 involve the O and OH radicals, which also play an important role in the oxidation of the fuel. Therefore, it is generally necessary to couple the thermal NO reactions with that of the fuel oxidation process. However, since the overall formation of NO is slow compared to the oxidation of fuel, it can be assumed, as first suggested by

Zel'dovich (Zel'dovich, 1946), that the thermal NO formation reactions can be decoupled from the fuel oxidation mechanism. Zel'dovich also said that the NO formation rates could be calculated assuming equilibrium values of temperature and concentrations of O_2, N_2, O, and OH. This is, therefore, known as the Zel'dovich mechanism (*cf.* Miller & Bowman, 1989).

1.1.2 Prompt NO_x mechanism

Prompt NO_x is NO that is formed at a rate faster than that calculated from the simple equilibrium thermal NO_x description (Zel'dovich mechanism). The formation of prompt NO_x is not fully understood. In general three sources of prompt NO_x can be distinguished; super equilibrium, Fenimore, and nitrous oxide mechanism.

Prompt NO_x can be a result of super equilibrium concentrations of O and OH in the reaction zone. This phenomenon can accelerate the rate of the Zel'dovich mechanism. This is because the Zel'dovich mechanism assumed that the reactions $\frac{1}{2}O_2 \rightleftharpoons O$ and $H + O_2 \rightleftharpoons OH + O$ are in partial equilibrium. Super equilibrium is most important in diffusion flames, stirred reactors at lean conditions, and low pressure premixed flames. It can account for as much as 80% of the NO formation in these flames (Drake & Blint, 1991).

The Fenimore prompt mechanism deals with the formation of NO in hydrocarbon flames by a reaction sequence that is initiated by hydrocarbon radicals, which attack nitrogen molecules. This leads to the formation of atomic nitrogen, cyanides and amines, which start a series of subsequent reactions to form NO. A number of species have been

suggested to be responsible for the prompt NO in hydrocarbon flames such as CH, CH_2, C_2, C_2H, and C (Miller & Bowman, 1989), however, the major contributors have been found to be CH, CH_2, and CN radicals. The mechanism is controlled by the following reactions,

$$\left.\begin{aligned} CH + N_2 &\rightleftharpoons HCN + N \\ N + OH &\rightleftharpoons NO + H \\ N + O_2 &\rightleftharpoons NO + O \end{aligned}\right\} \quad (1.8)$$

$$\left.\begin{aligned} CH_2 + N_2 &\rightleftharpoons HCN + NH \\ NH + H &\rightleftharpoons N + H_2 \\ N + OH &\rightleftharpoons NO + H \\ N + O_2 &\rightleftharpoons NO + O \end{aligned}\right\} \quad (1.9)$$

$$\left.\begin{aligned} CN + O_2 &\rightleftharpoons OCN + O \\ ONN + O &\rightleftharpoons CO + NO \end{aligned}\right\} \quad (1.10)$$

$$\left.\begin{aligned} CN + H_2 &\rightleftharpoons HCN + H \\ CN + H_2O &\rightleftharpoons HCN + OH \\ NH + H &\rightleftharpoons N + H_2 \\ N + O_2 &\rightleftharpoons NO + O \\ N + OH &\rightleftharpoons NO + H \end{aligned}\right\} \quad (1.11)$$

Reactions 1.8 was first suggested by Fenimore (Fenimore, 1971), hence the name Fenimore prompt mechanism. This is the most dominate step in then Fenimore mechanism. The Fenimore mechanism dominates in fuel rich premixed flames and is also important in diffusion flames.

The third prompt mechanism is the nitrous oxide mechanism. This mechanism concerns the reactions between N_2O and O. The nitrous oxide pathway is given below by reactions 1.12-1.19. The mechanism is initiated by the reverse reaction of 1.12, at which time the N_2O formed is oxidized to NO primarily by reaction 1.13. However, NO can also be formed by reactions 1.14-1.16. The remaining N_2O is then reduced by reactions 1.12 and 1.17-1.19 (Bonturi et al., 1996).

$$N_2O + M \rightleftharpoons N_2 + O + M \quad (1.12)$$

$$N_2O + O \rightleftharpoons NO + NO \quad (1.13)$$

$$N_2O + H \rightleftharpoons NO + NH \quad (1.14)$$

$$N_2O + CO \rightleftharpoons NO + NCO \quad (1.15)$$

$$N_2O + M \rightleftharpoons N + NO + M \quad (1.16)$$

$$N_2O + O \rightleftharpoons N_2 + O_2 \quad (1.17)$$

$$N_2O + H \rightleftharpoons N_2 + OH \quad (1.18)$$

$$N_2O + OH \rightleftharpoons N_2 + HO_2 \quad (1.19)$$

The N_2O-O mechanism becomes more important in very lean flames, and low temperatures, and is enhanced by super-equilibrium O atom concentrations. It is also very important at high pressures because the high pressure facilitates a higher probability of a three body reaction.

1.1.3 Fuel Bound NO_x

Another important contributor to NO_x production is nitrogen that is bound chemically to the fuel. This can be the primary source of NO_x emissions from the combustion of fossil fuels. Fuels such as ammonia (NH_3) or pyridine (C_5H_5N) break apart during the oxidation process and leave N-atoms free to react with O-atoms. The extent to which the N converts to NO is a strong function of the temperature and the fuel-to-air ratio. It is also a strong function of the fuel nitrogen content. However, it is nearly independent of the composition of the parent fuel molecule.

Song et al. (1981), through kinetic modeling, and Chen et al. (1982), through laboratory experiments, showed that at $\phi > 1$ the conversion of fuel nitrogen to NO is less prevalent than for $\phi \leq 1$. Some of the NO formed under this mechanism may react with smaller hydrocarbon radicals. This facilitates the conversion of NO, formed during the combustion process, to cyano compounds (HCN or CN). Under fuel-rich conditions these compounds may react to form N_2. This mechanism has many common features with the Fenimore mechanism, i.e., HCN formation (Bowman 1992).

1.1.4 NO_2 Reaction Mechanism

A significant source of NO_x can be attributed to nitrogen dioxide, NO_2. NO_2 is mainly formed by the reactions of NO with HO_2, OH, O, and O_2 by the following reactions,

$$NO + HO_2 \rightleftharpoons NO_2 + OH \tag{1.20}$$

$$NO + OH \rightleftharpoons NO_2 + H \tag{1.21}$$

$$NO + O_2 \rightleftharpoons NO_2 + O \tag{1.22}$$

$$NO + O + M \rightleftharpoons NO_2 + M \tag{1.23}$$

Because of its short lifetime in high temperature zones most NO_2 formation occurs in the low temperature regions of the flame. Here significant amounts of HO_2 can be found to react with NO formed in high temperature regions that are transported to the low temperature regions by diffusion. Since NO_2 is sensitive to the HO_2 present in low temperature regions of the flame, as shown in equation 1.20, it is also sensitive to reactions responsible for the formation and destruction of HO_2. The most important reaction for the formation of HO_2 in low temperature zones is,

$$H + O_2 + M \rightleftharpoons HO_2 + M \tag{1.24}$$

The H-atoms needed for this reaction also come from the high temperature zone by diffusion (Miller & Bowman, 1989).

For counterflow diffusion flames the mechanisms that are most important are the thermal mechanism, Fennimore prompt mechanism, and the Super equilibrium mechanism.

1.2 Flamelet Theory

Turbulent diffusion flames have a very complex flame surface caused by turbulent eddies which cause the flame to distort and wrinkle at the large scale and augment the diffusional transport at the small scales. In order to better understand turbulent diffusion flames flamelet theory was developed to describe the response of these complex flame fronts to the non-equilibrium effects of turbulence and the resulting chemical kinetics.

Flamelet theory treats the complex flame structure of the turbulent diffusion flame as an ensemble of strained, laminar, one dimensional flamelets as shown in Figure 1.1.

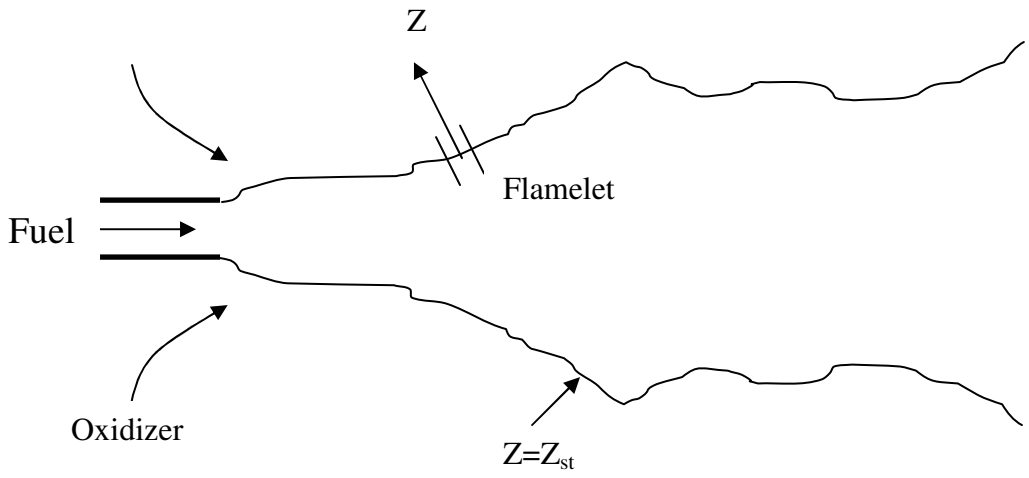

Figure 1.1 Representation of a turbulent diffusion flame illustrating a diffusion flamelet

Burke and Schumann (1928) were the first to characterize a diffusion flame using a conserved scalar. They suggested that the Damköhler number (Da), the ratio of fluid dynamic time to chemical kinetic time, was infinite. The Da = ∞ assumption implies that the flame is a one-dimensional stoichiometric surface. They also assumed single step chemistry and a Lewis number (Le), the ratio of heat and mass diffusivities, equal to unity.

Flamelet theory says that all temperature and species profiles for the 1-D flamelet can be completely described by a single conserved scalar for Da = ∞, Le = 1, and single step chemistry. The conserved scalar used is the mixture fraction, Z, which is a function of the fuel mass fraction and is bounded between zero, for pure air, and unity, for pure fuel.

$$Z = \frac{\beta - \beta_{O,0}}{\beta_{F,0} - \beta_{O,0}}$$

$$\text{where} \quad \beta = \frac{Y_O}{M_O(\nu''_O - \nu'_O)} - \frac{Y_F}{M_F(\nu''_F - \nu'_F)} \tag{1.25}$$

Y_O is the mass fraction of the oxidizer, Y_F is the mass fraction of the fuel, M is the molecular weight, ν' and ν'' are the stoichiometric coefficients for the reactants and products, respectively. Using this analysis, Burke and Schumann were able to predict flame shape and height reasonable well, for the first time. One advantage of this method is that temperature and species profiles are linear in mixture fraction space.

In diffusion flames the mixture fraction is continuously changing throughout the flowfield, and can be expressed as a function of the equivalence ratio. Assuming fast chemistry, the flame is infinitely thin and exists at the stoichiometric mixture fraction contour. The stoichiometric mixture fraction is given by,

$$Z_{st} = \left(1 + \frac{Y_{F,1} \cdot \nu'_O \cdot M_O}{Y_{O,2} \cdot \nu'_F \cdot M_F} \right)^{-1} \tag{1.26}$$

In order to predict phenomena such as flame quenching, liftoff and blowoff, and pollutant formation the non-equilibrium effects of finite rate chemistry must be included. With finite rate chemistry the flame is no longer one-dimensional, but is now of finite thickness, which is modeled as a diffusive-reactive zone. In order to account for non-equilibrium effects an additional variable, χ, the instantaneous scalar dissipation rate, must be introduced.

$$\chi \equiv 2D\left|\Delta Z\right|^2 \tag{1.27}$$

where D is the diffusion coefficient.

The scalar dissipation rate can be interpreted as the inverse of a characteristic diffusion time and due to the transformation that leads to this parameter, it incorporates the effects of convection and diffusion normal to the surface of the stoichiometric mixture (Peters, 1984 & 1986). The scalar dissipation rate varies inversely with Damköhler number, so as the fluid transport time gets shorter (increasing strain rate), the dissipation rate increases. The scalar dissipation rate is a measure of the heat conduction from both sides of the diffusive-reactive zone.

The governing equation in the region of the reactive – diffusive zone can be written as,

$$\frac{d^2\hat{y}}{d\xi^2} = \delta(\hat{y}^2 - \xi^2)e^{-(\hat{y}+\gamma\xi)} \tag{1.28}$$

where $\hat{y}$ is the scaled mass fraction, ξ is the stretched mixture fraction variable, δ is the reduced Damköhler number, and γ is a non-dimensional temperature. The scaled mass fraction, stretched mixture fraction, reduced Damköhler number, and non-dimensional temperature are given by,

$$\hat{y} = \frac{(T_{st} - T)E_a}{R_u T_{st}^2} - \gamma\xi \text{ , where } E_a \text{ is the activation energy} \tag{1.29}$$

$$\xi \equiv \beta(Z - Z_{st}) \tag{1.30}$$

$$\delta = \frac{Y_{0,O}A_F e^{(-E_a/R_u T_{st})}}{2\rho D\left|\Delta Z_{st}\right|^2 Z_{st}\beta^3} \text{ , where } A_F \text{ is the rate constant for the consumption of fuel} \tag{1.31}$$

$$\gamma \equiv ZZ_{st} - 1 - ZZ_{st}(1 - Z_{st})\left\{\frac{T_{F,0} - T_{o,0}}{T_{st} - T_c}\right\} \text{ , where } T_c \text{ is the cold flow temperature} \tag{1.32}$$

For a given γ the governing equation can be numerically integrated to yield the maximum temperature as a function of the reduced Damköhler number, δ. This is shown in the S-curve in Figure 1.2. Thus if χ is increased past a critical value, χ_q, then the amount of heat conducted away from the reaction zone exceeds the amount of heat generated by the chemical reaction and the flame quenches. If equation 1.26 is evaluated at a value of Z at the stoichiometric surface, Z_{st}, the result is the stoichiometric scalar dissipation rate, χ_{st}.

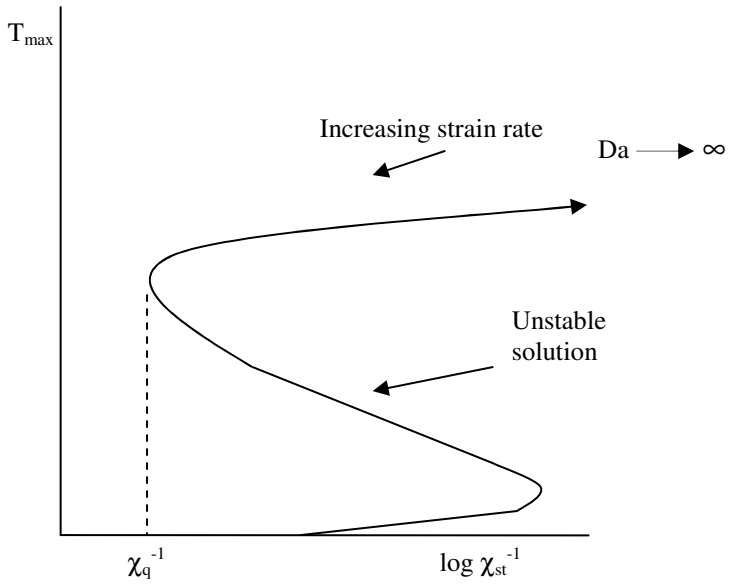

Figure 1.2 The S-shaped curve showing the quenching scalar dissipation rate.

The two-parameter formulation assumes the flamelet responds in a quasi-steady manner to unsteady hydrodynamics. However, recent experimental and numerical results show that the application of unsteady strain rates to a laminar flamelet will result in a transient response (Im et al., 1995; Welle et al., 2002).

1.3 Counterflow Diffusion Flames

A burner comprised two opposed jets containing fuel and oxidizer impinging on a stagnation surface is know as a counterflow diffusion flame (CFDF). A CFDF has many essential features of a laminar diffusion flamelet and has the advantage of being very repeatable. CFDF's have been used extensively to study, both experimentally and computationally, hydrogen and light hydrocarbons flowing against air, with and without dilution. The burner used in this study is similar to the design of Seshadri (Puri & Seshadri, 1986), but modified to generate an unsteady flow field (Riggen-DeCroix, 1998).

Figure 1.3 is a sketch showing a counterflow diffusion flame stabilized near the stagnation plane of two steady, laminar opposed jets of fuel and oxidizer. For momentum-matched opposed jets the axial velocity gradient (strain rate) is given by,

$$a = \frac{2V_o}{L}\left[1 + \frac{V_f}{V_o}\left(\frac{\rho_f}{\rho_o}\right)^{0.5}\right], [s^{-1}] \tag{1.33}$$

where a is the strain rate and V_o, V_f, ρ_f, ρ_o and L are the oxidizer outlet velocity, fuel outlet velocity, fuel density, oxidizer density and burner separation distance, respectively (Seshadri and Williams, 1978). In this study the global strain rate (GSR) is defined as (Riggen-DeCroix, 1998),

$$a = \frac{2V_o}{L} \tag{1.34}$$

Peters (2000) derived the scalar dissipation rate along the stoichiometric mixture fraction contour for stagnation point flow, which is a function of the strain rate, a,

$$\chi(Z_{st}) = \frac{2a}{\pi}\exp\left[-2\cdot(erf^{-1}[2\cdot Z_{st}]^2)\right] \tag{1.35}$$

The scalar dissipation rate is a fundamental parameter as it describes the molecular mixing and couples the reaction zone response to the flow field. Also, this relationship is

important because it relates the scalar dissipation rate to an easily measured quantity, the strain rate a.

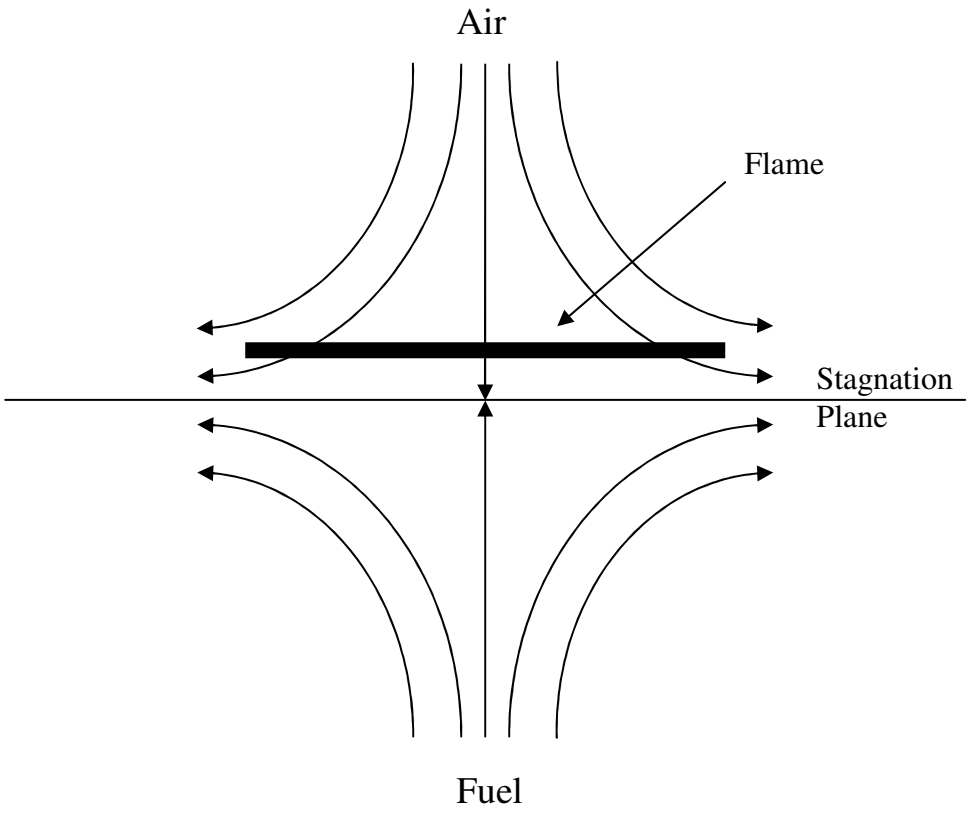

Figure 1.3 Sketch of a stagnation point flow field in a counterflow diffusion flame

For flamelets subjected to unsteady strain rates, the scalar dissipation rate is time dependent. Recent experimentation (DeCroix et al., 1998; Welle et al., 2000) and computational results (Im, et al. 1995; Pitsch et al., 1998; Im, et al., 1999) has show that these unsteady flamelets do not respond quasi-steadily as earlier expected. In fact as the mean χ approaches the critical value, the instantaneous scalar dissipation rate may actually exceed χ_q for short periods of time. The two parameter flamelet model, however, cannot account this transient effect.

2 Description of Experimental Apparatus

2.1 Counterflow Diffusion Flame Burner

Figure 2.1 is a schematic of the counterflow diffusion flame burner used in this experiment. The burner is similar to that described by Seshadri (Puri & Seshadri, 1986), but has been modified to generate an unsteady flow.

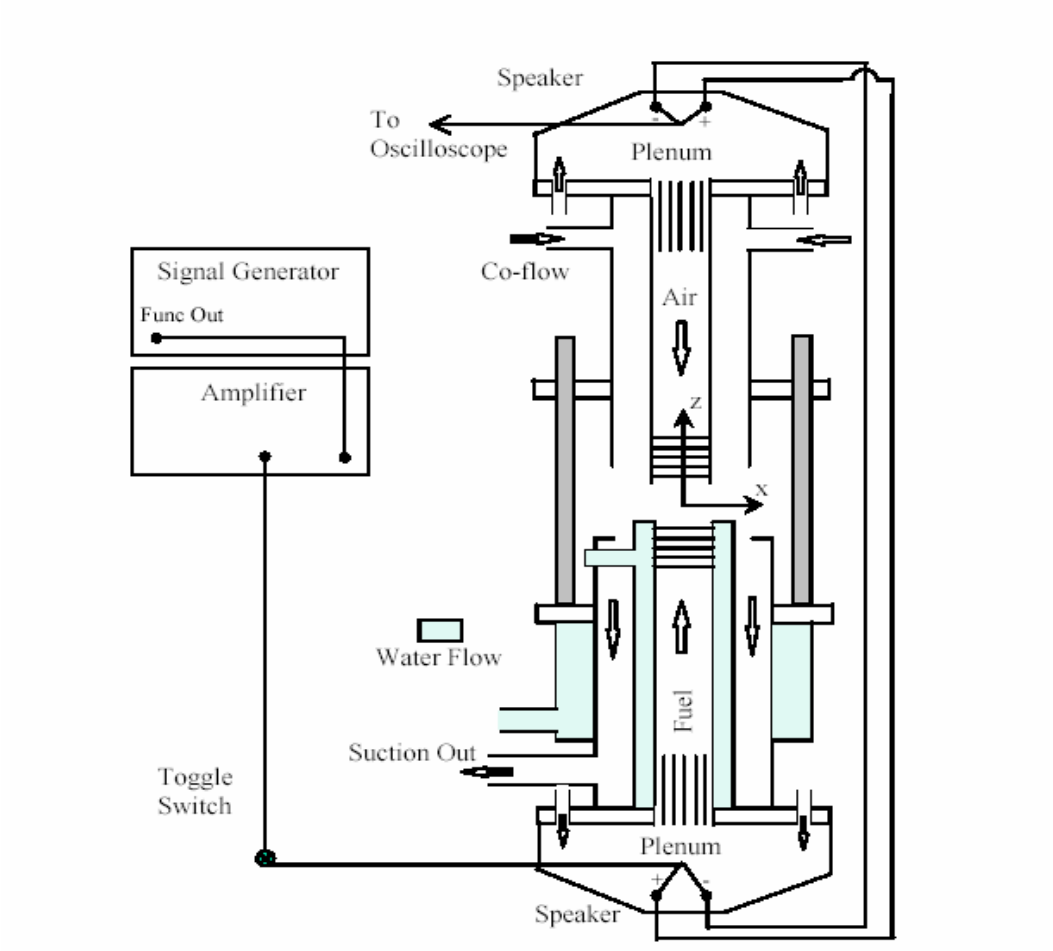

Figure 2.1 Schematic of counterflow diffusion flame burner

The counterflow burner was operated at atmospheric pressure. The reactants flow through 2.54 cm diameter tubes centered in the top (oxidizer side) and bottom (fuel side) sides of the burner. The separation distance of the fuel and oxidizer tubes was held constant at 1.27cm.

The oxidizer tube was surrounded by a 0.6 cm thick annulus for a nitrogen coflow. This prevented preheating of the oxidizer and entrainment of ambient air into the reaction zone. The velocity of the nitrogen coflow was set to match that of the air. The fuel tube was surrounded by an inner water jacket to prevent preheating of the fuel. A heat exchanger was used to cool the exhaust gases down to room temperature and prevent preheating of the fuel. Combustion products were pumped from the test section through an annulus by a shop-vac connected to the burner. For these experiments the suction of the vacuum was set to 1.5 inches of water.

A 25 mesh screen was laid across the entrance of the exhaust tube to stabilize the flame. Since the flame attached itself to the screen so there was soot deposits on the screen. For highly sooting fuels or long running times measured NO_x values began to drift due to large deposits of soot on the screen. For this reason the screen was cleaned often.

Five one inch, 100 mesh steel screens, separated by 3mm spacers were placed in the reactant delivery tubes. The screens flattened the exit velocity profile to be similar to a top hat profile. Each screen was oriented at a 45° to the one above and below it. It was found that to achieve the best results the screen at the exit of the tube needs to be a 150 mesh screen.

The unsteady flow field was imposed by using two 20cm Kicker C8a subwoofer loudspeakers (Riggen-DeCroix, 1998). The fluctuation in the delivered fuel and oxidizer

was set up by applying a sine wave of know frequency and amplitude to the speakers. The sine wave was generated by a SRS Model DS335 signal generator. A McIntosh amplifier was connected between the signal generator and the speakers to provide a 2:1 amplification for large amplitudes. The speaker signal was monitored with an oscilloscope. A photograph of the CFDF burner is shown in Figure 2.2.

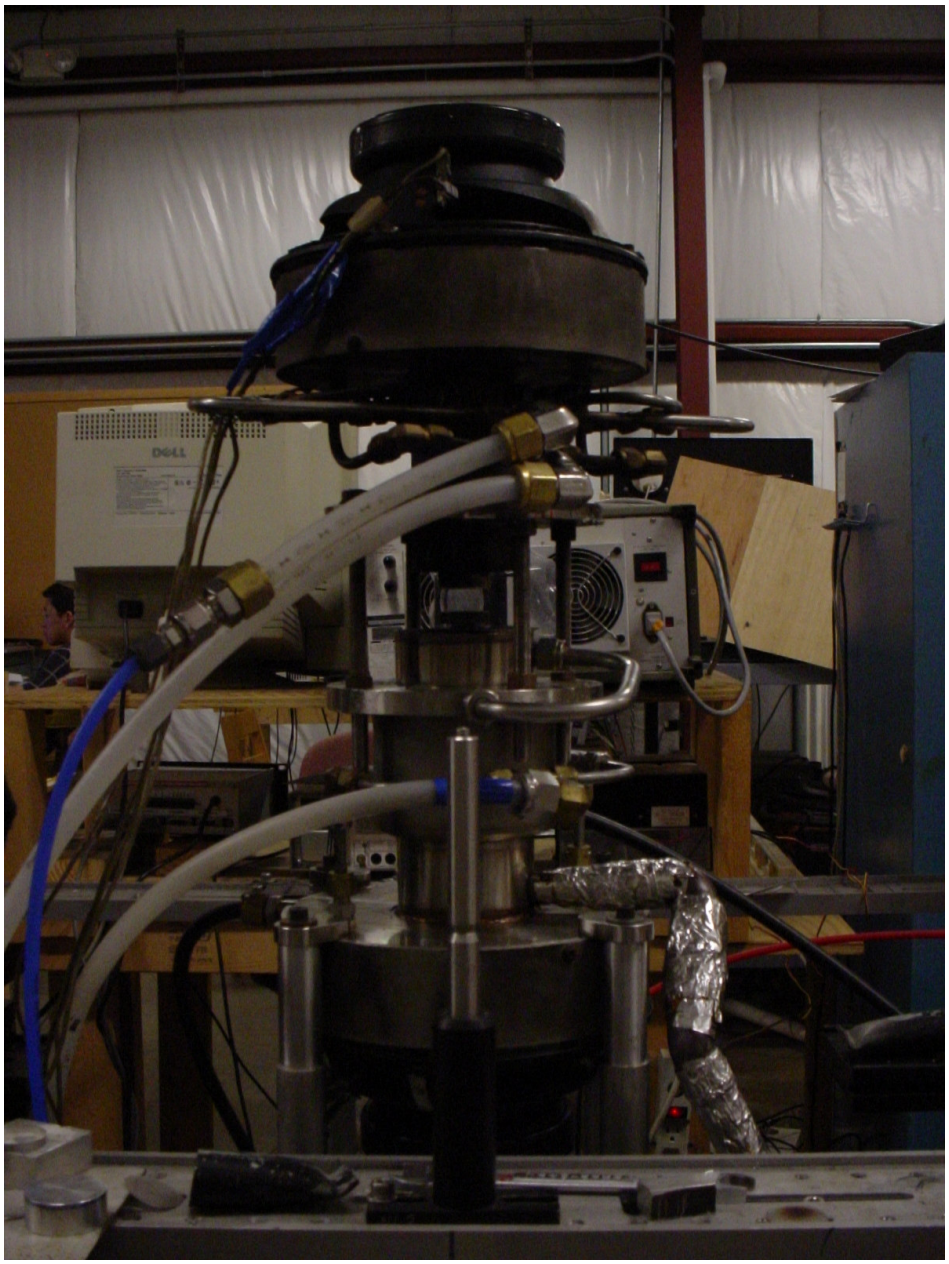

Figure 2.2 – Counterflow diffusion flame burner used in experiments

2.2 NO_x Analyzer

Measurements of both NO and NO_x were taken using a California Analytical Instruments Model 400 HCLD NO/NO_x analyzer (shown in Figure 2.3) as a function of fuel type, strain rate, and amplitude/frequency of imposed oscillation. The Model 400 HCLD uses chemiluminescence to analyze the NO or NO_x concentration within a gaseous sample. It has two selectable modes NO and NO_x. In the NO mode the analyzer measures the concentration of NO in the sample and in the NO_x mode it measures the concentration of NO + NO_2. A t-joint was installed down stream of the heat exchanger so the analyzer could draw sample gases from the CFDF exhaust line.

Figure 2.3 – California Analytical Instruments Model 400 HCLD NO/NO_x analyzer used in experiments.

The California Analytical Instruments Model 400 HCLD Analyzer utilizes the principle of chemiluminescence for analyzing the NO or NO_x concentration within a gaseous sample. In the NO mode, the method is based upon the chemiluminescent reaction between ozone and nitric oxide (NO) yielding nitrogen dioxide (NO_2) and oxygen.

Approximately 10% of the NO_2 produced from this reaction is in an electronically excited state. The transition from this excited state back down to a ground state produces a photon, and the intensity is proportional to the number density of NO_2 in the reaction chamber. The light is measured by means of a photodiode tube and associated amplification electronics. In the NO_x mode, NO plus NO_2 is determined as above, however, the sample is first routed through the internal NO_2 to NO converter which converts the NO_2 in the sample to NO. The resultant reaction is then directly proportional to the total concentration of NO_x. The entire sample, prior to the reaction chamber, is maintained at a temperature of 65°C.

3 Numerical Method

The numerical results for the steady flow field were obtained using OPPDIF (Lutz et al., 1996). OPPDIF is a FORTRAN program that computes the diffusion flame between two opposing nozzles. The two-dimensional axisymmetric flow field is reduced to a one-dimensional problem using a similarity transform. Assuming that the radial component of velocity is linear in radius, the dependent variables become functions of the axial direction only. OPPDIF solves for the temperature, species mass fractions, axial and radial velocity components, and radial pressure gradient, which is an eigenvalue in the problem. The Twopnt software solves the two-point boundary value problem for the steady-state form of the discredited equations (Lutz et al., 1996). The Chemkin packages are used to calculate the chemical reaction rates and thermodynamic/transport properties. The chemical mechanism used was GRI-mech 3.0 (listed in appendix 8.5) with its corresponding thermodynamic and transport properties. Flame profiles for the species mass fraction were spatially integrated to obtain equilibrium values for which could be compared to data obtained from the gas analyzer. The emission index is also output by the code.

The numerical results for unsteady flow fields were computed using OPUS (Im et al., 2000). OPUS is a FORTRAN program for computing unsteady combustion problems in an opposed flow configuration using one-dimensional similarity coordinate. The code is an extension of its steady counterpart, OPPDIF, to handle unsteady strain rates by modifying the formulation to accommodate, gas dynamic compressibility effects. This allows high-accuracy time integration with adaptive time stepping. Time integration of the differential-algebraic system (DAE) of equations is performed by the DASPK software package. DASPK replaces the OPPDIF Newton solver, Twopnt, and is a solution package

for solving the DAE's. DASPK incorporates a variable-order, variable-step backward-differentiation formula to solve the DAE's. This allows for a robust time integration of complex unsteady problems. Like the steady code OPPDIF, OPUS also uses the Chemkin packages to compute the associated chemical reaction rates and thermodynamic/transport properties (Im et. al, 2000).

In order to accurately match the experimental velocity oscillation pattern the function that described the unsteady velocity profile had to be rewritten. Originally the code described the velocity as,

$$u(t) = U_{steady} \times \left[1 + AMP\{1 - \cos(2\pi ft)\}\right]$$

However, when the function was changed to

$$u(t) = U_{steady} \times \left[1 + AMP \sin(2\pi ft)\right],$$

the code became unstable and crashed on the first time step. After much trial and error, it was decided that, in order to get around this problem the amplitude needed to gradually increase to its desired value. To do this, a form of the hyperbolic tangent was incorporated into the forcing function. After a measure of time the hyperbolic tangent would go to unity, leaving just the sin function. Therefore, the function used was:

$$u(t) = U_{steady} \times \left[AMP \left(\frac{e^{2t^3} - 1}{e^{2t^3} + 1} \right)^{1/2} \sin(2\pi ft) \right]$$

This allowed the function to reach its desired value much faster than a normal hyperbolic tangent function. This function is compared to a regular sine wave in Fig. 3.1. The modified code is listed in Appendix 8.4.

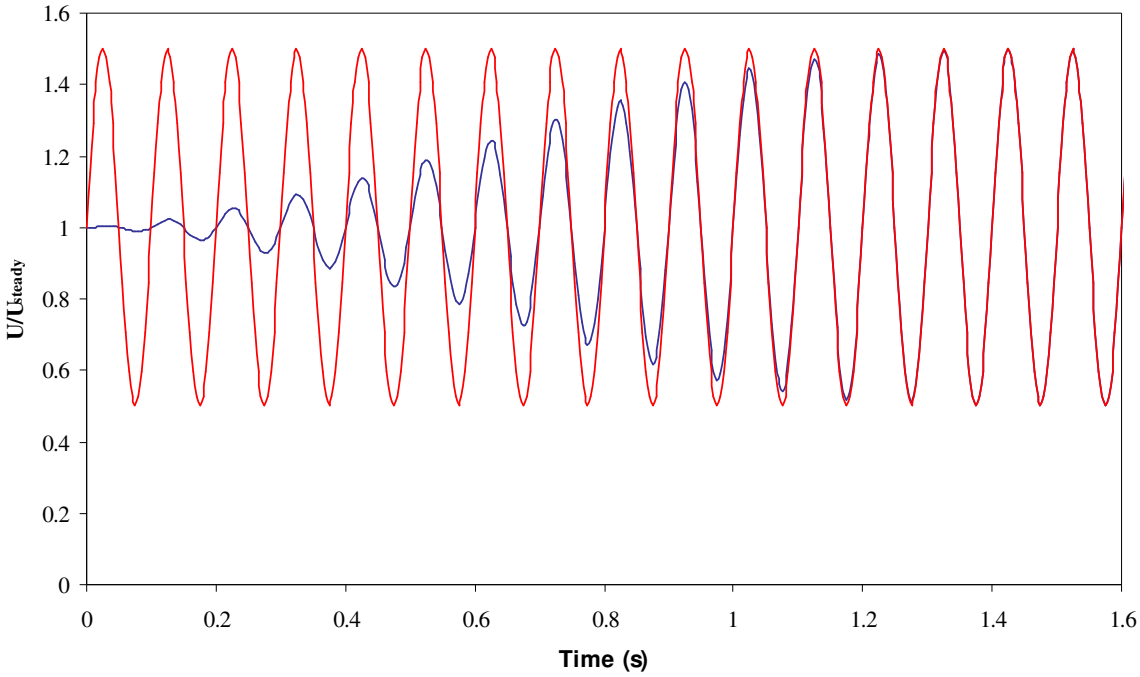

Figure 3.1 - Comparison of speaker induced velocity oscillations and that of the opus code.

OPUS outputs species mass fractions, maximum temperature, and emission indices as a function of time. It was also modified to output the overall species concentrations. From this the time average values can be calculated and compared to experimental values. This modification is listed in Appendix 8.3.

4 Steady Counterflow Diffusion Flames

Readings of NO and NO_x ($NO + NO_2$) were taken for strain rates of 30, 60, 90, 120, and 150 s^{-1} for methane, propane, and initially ethylene. Initial measurements for steady state methane and propane flames show that the NO_x concentration increased with strain rate as seen in Figure 4.1. This appears to run counter to what was expected so certain steps were taken in order to validate the experimental data.

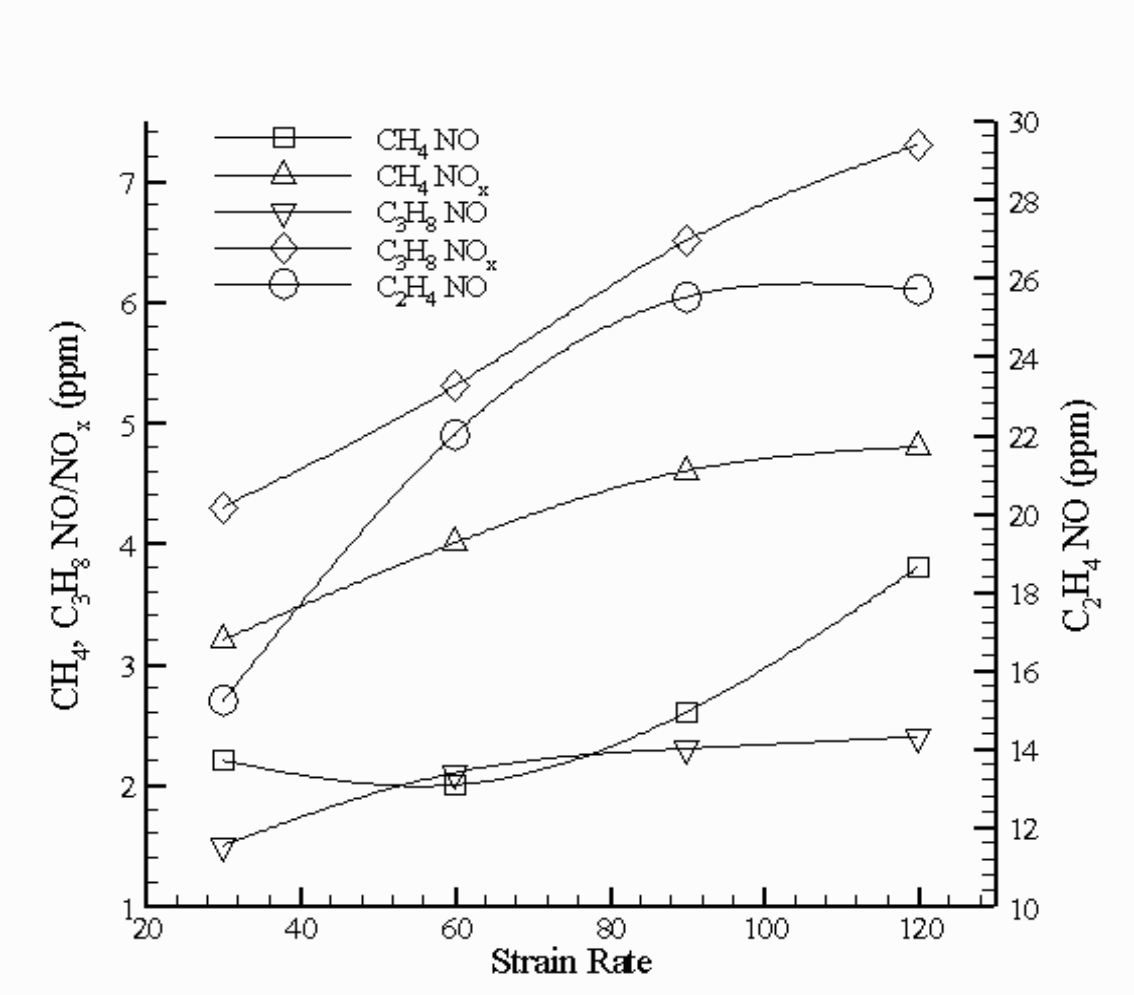

Figure 4.1 Uncorrected measured NO and NO_x concentration versus steady strain rate. CH_4 and C_3H_8 are plotted on the left axis while C_2H_4 is plotted on the right axis due to the very high soot loading associated with ethylene.

The first step was to express the NO_x concentration in terms of the emission index, EI. The emission index is the ratio of the mass rate of NO/NO_x produced per mass flux of fuel supplied. The emission index is give by:

$$EI_{NO} = \frac{\dot{m}_{NO}}{\dot{m}_F} = \frac{\dot{m}_{NO}}{\rho_F u_F \pi d^2 / 4}, \text{ [g/kg]} \tag{4.1}$$

where ρ_F is the fuel density, u_F is the fuel velocity and d is the diameter of the exit tube. In order to calculate $\dot{m}_{NO}$ it was important to express it in terms of the mole fraction of NO, which is easily obtained from experimentation:

$$\dot{m}_{NO} = \dot{V}_{NO}\rho_{NO} = X_{NO}\dot{V}_{products} \tag{4.2}$$

From the conservation of mass it is clear that, $\dot{V}_{products}$ (slpm) is equal to the sum of the volume flow rates of the fuel, oxidizer, and nitrogen coflow, corrected for standard temperature and pressure, if the number of moles are equal.

In order to accurately calculate the volume flow rates of the products it was important to be sure that no room air was being entrained into the flame or exhaust tube due to the low pressure annulus around the fuel tube. To do this, the burner test section was enclosed with aluminum tape, as shown in Figure 4.2. This ensured that $\dot{V}_{products}$ was in fact equal to $\dot{V}_F + \dot{V}_O + \dot{V}_{N_2 coflow}$.

1. Upon repeating the experiments with the enclosure, the data was seen to drastically change from the previous results. Five runs, at each strain rate, were completed and the error bars show that the data is very repeatable. Figure 4.3 shows the new experimental data for C_3H_8 and CH_4. At high steady strain rates the NO concentration, for propane, decreases with increasing steady strain rate except between 30 and 60 s^{-1}. Here the opposite is true due to high soot loading, and thus, high radiative hear transfer. The NO_x

concentration increases with steady strain rate, which show that more NO_2 is produced at high strain rates.

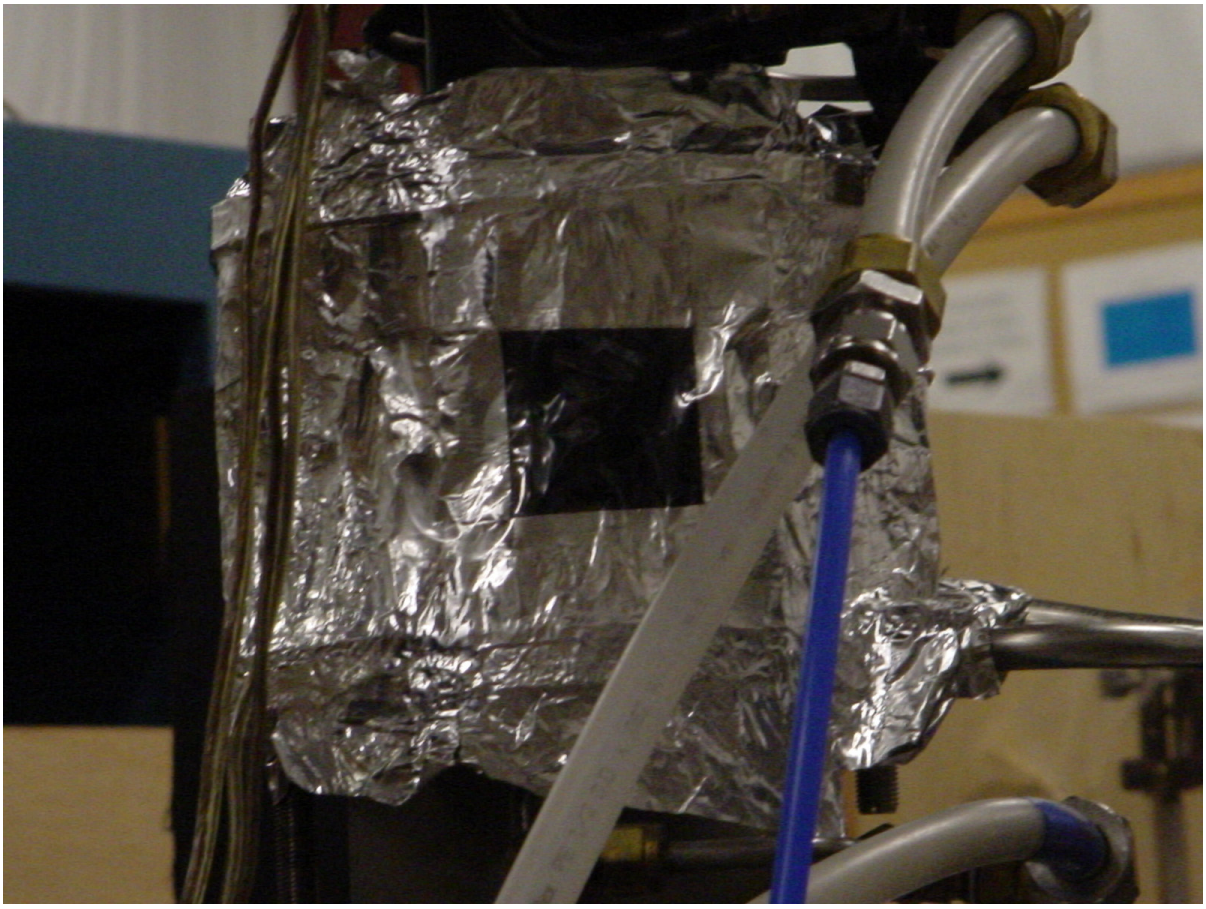

Figure 4.2 – Counterflow diffusion flame burner with the test section shielded from room air with a window built in for flame observation.

For methane, instead of increasing with strain rate, the NO concentration now decreases with increasing strain rate as expected. The NO_x concentration also decreases with steady strain rate except between 30 and 60 Hz. This is the result that would be expected since the flame temperature also decreases with increasing strain rate. Experiments for C_2H_4 were not repeated because its high flame temperature began to melt the speakers mounted on the burner.

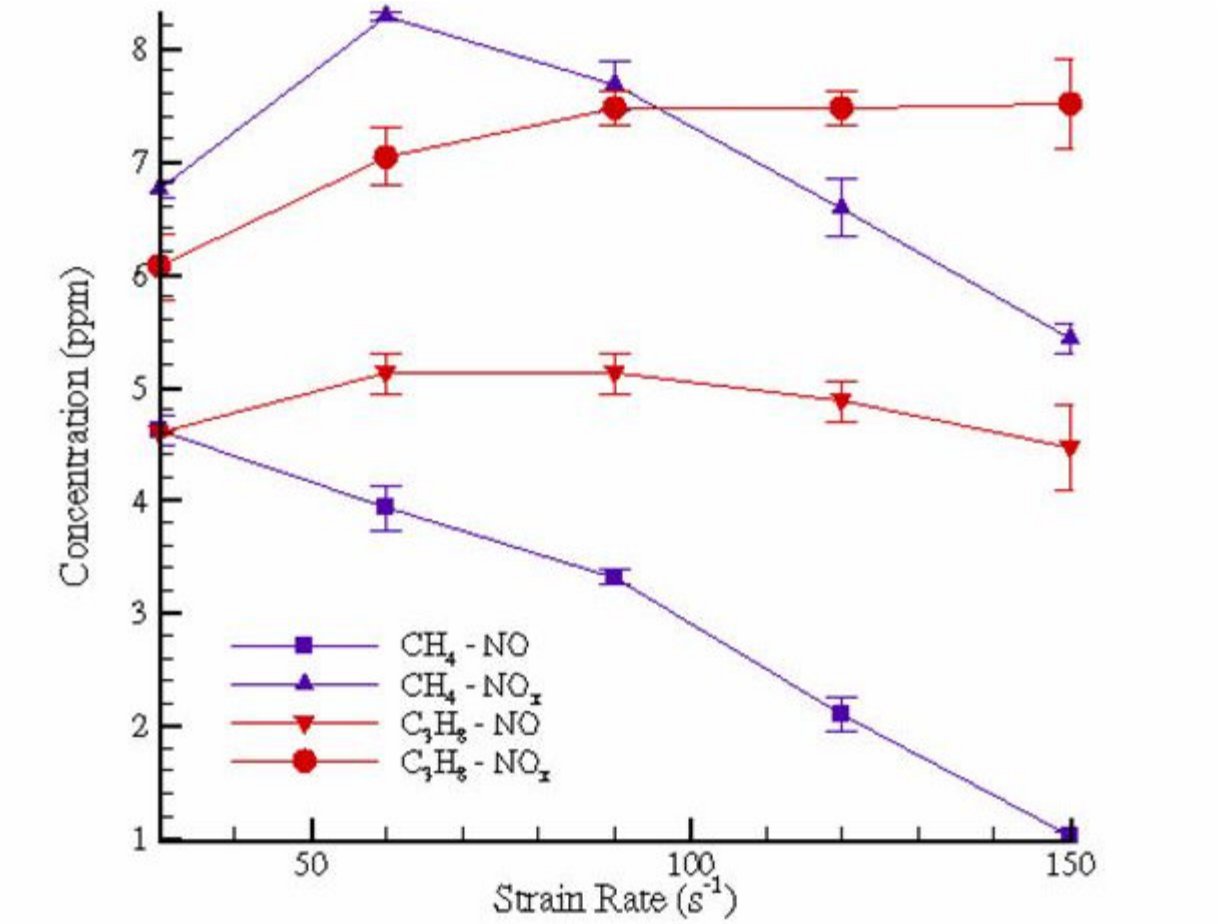

Figure 4.3 – Measured steady NO and NO_x concentration in ppm versus steady strain rate for C_3H_8 and CH_4.

Figure 4.4 shows the comparison between OPPDIF results and experimental data for a methane-air flame. The experimental results matched the numerical results very well for NO at high strain rates. However at low strain rates, particularly 30 s^{-1}, experiment and computation diverge. At a strain rate of 30 s^{-1} computational results predict twice as much NO formation over what was experimentally measured. Even though methane is a low sooting fuel, soot is still present at the lower strain rates, causing some of the heat to be radiated away from the reaction zone. As the strain rate increases, the residence time of incipient soot particles in the high temperature zone is reduced and the total amount of soot decreases dramatically. Experimental data shows that NO_2 has

a significant contribution to the total NO_x production, while the numerical results show virtually no NO_2.

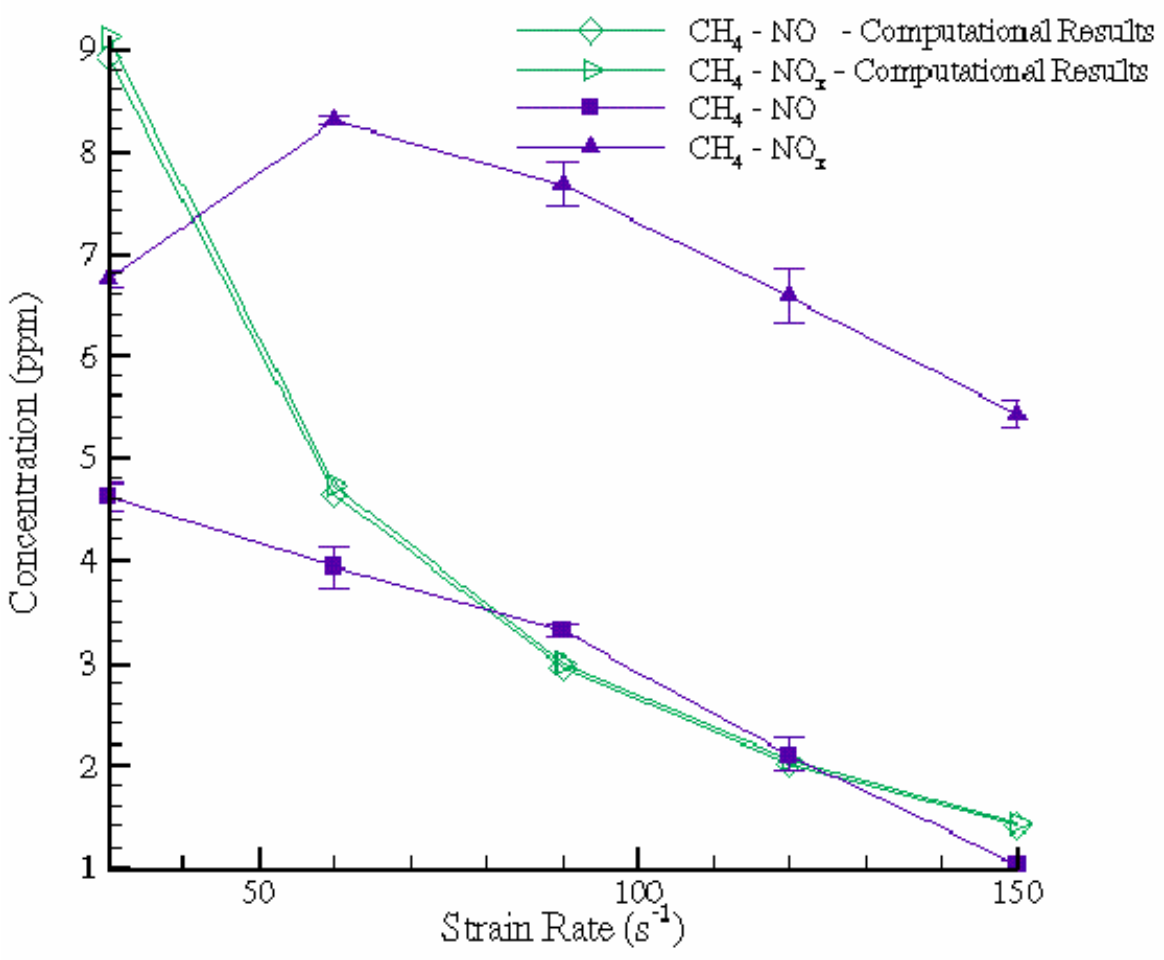

Figure 4.4 – NO and NO_x concentration versus strain rate for the modified burner. Both numerical and experimental results for CH_4 are plotted.

The emission index was also calculated and plotted for varying strain rates. Figure 4.5 shows how the emission index of NO (EI_{NO}) varies with steady strain rate for both the experimental data for C_3H_8 and CH_4. Here the NO emission index drops slightly with increasing steady strain rate, while the NO_x emission index remains relatively constant with increasing steady strain rate.

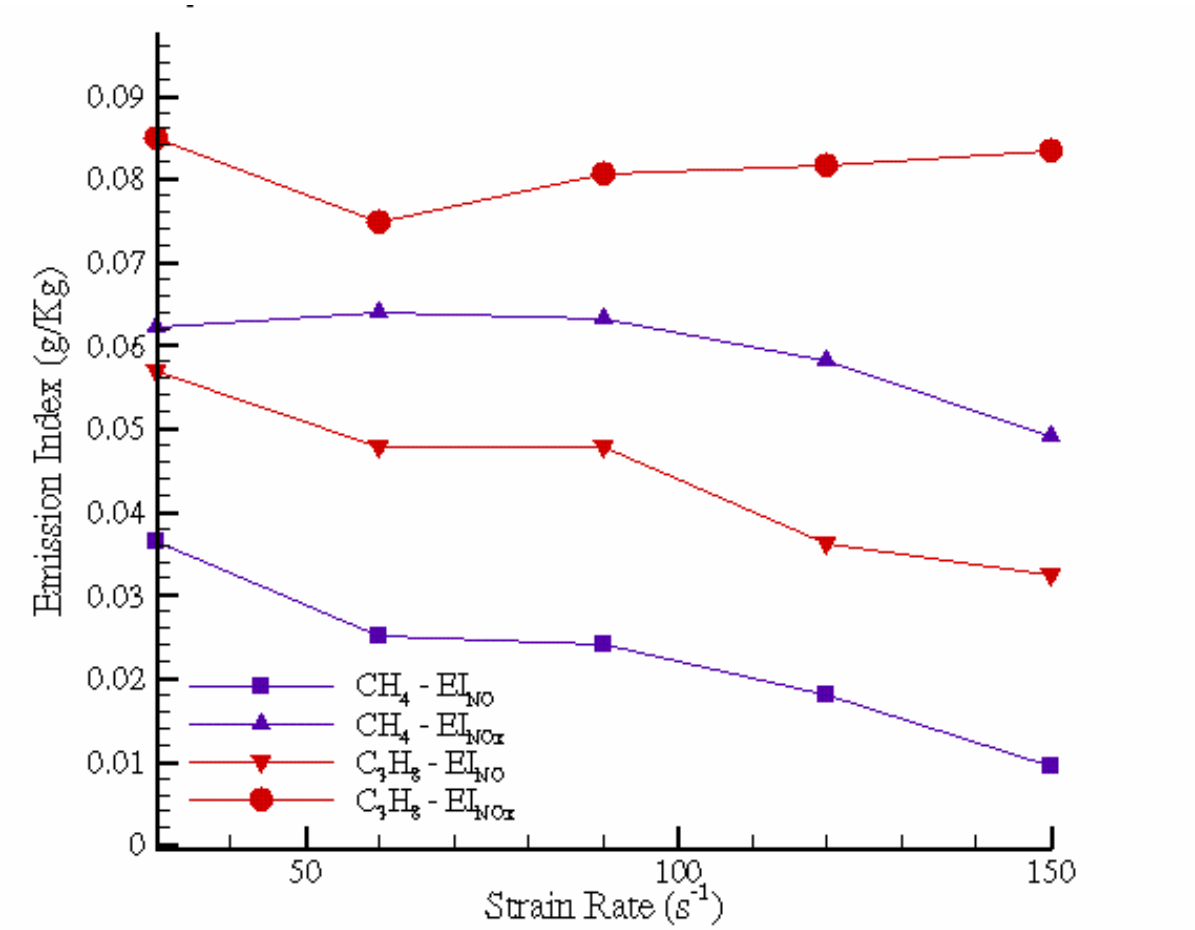

Figure 4.5 - Measured NO and NO_x emission index for varying steady strain rates for C_3H_8 and CH_4.

Figure 4.6 shows how both EI_{NO} and EI_{NOx} vary with steady strain rate for experimental and computational results for CH_4. Both EI_{NO} and EI_{NOx} for the computational data are considerably higher than their experimental counterparts. The slope of the EI_{NO} curve from the experimental data is much steeper than that of the predicted values. The absolute slope of the numerical curve is 7.2×10^{-3}, and the experimental is 1.83×10^{-4}. This is a substantial difference. The numerical emission index values are in good agreement with the numerical results presented by Nishioka et al. (1994). The experimental emission index was calculated using the method described

above, while the computational emission index uses the molar production rates, similar to that outlined by Turns (1995).

It is interesting to note contribution of NO_2 to the total EI_{NOx}. As with the concentration data the experimental EI_{NOx} has a large contribution of NO_2, while the computed values hardly has any contribution of NO_2 to the total NO_x.

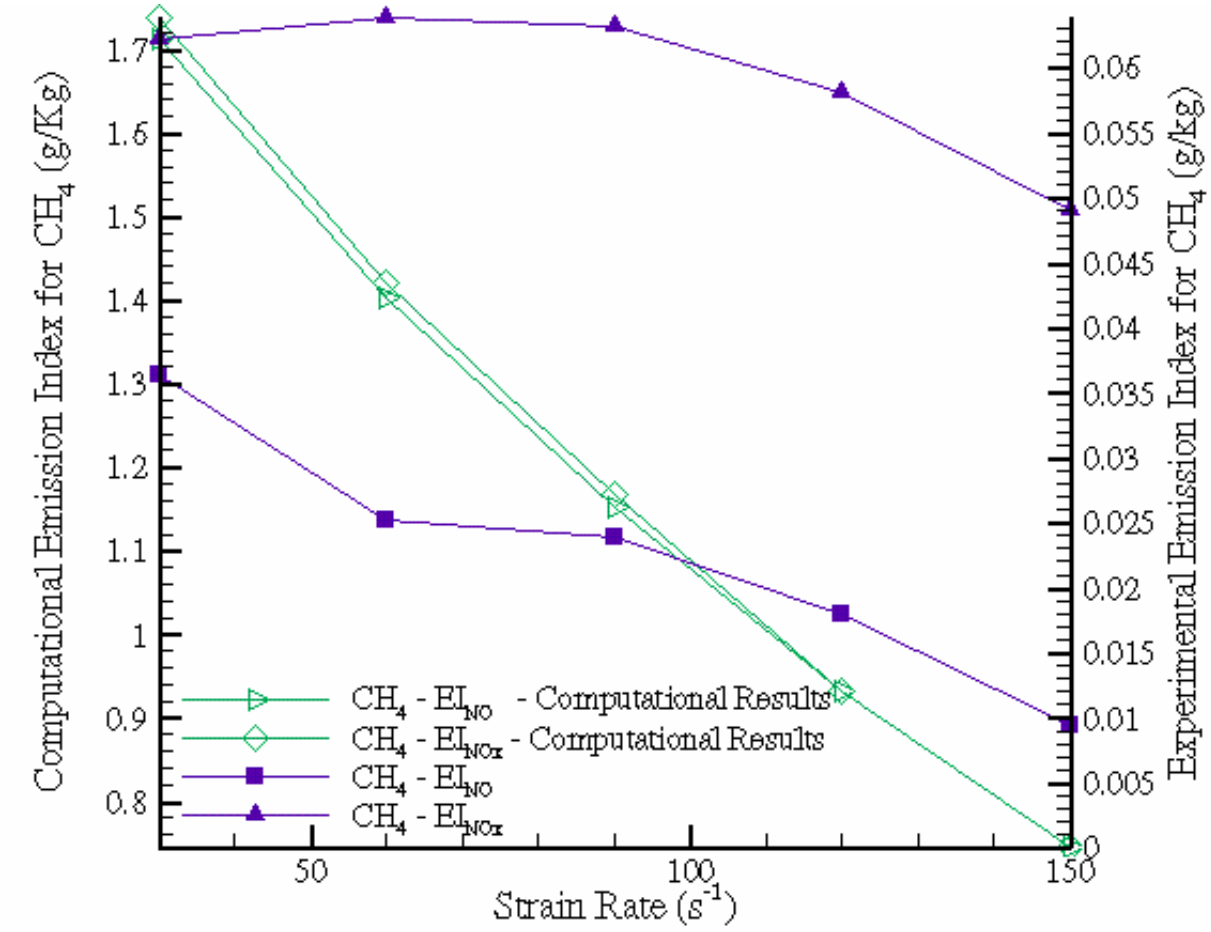

Figure 4.6 - NO emission index for varying steady strain rates for CH_4. Experimental data is plotted the right axis and numerical results are plotted on the left axis.

5 Unsteady Counterflow Diffusion Flame

Measurements for the unsteady counterflow diffusion flames were also taken at global strain rates of 30, 60, 90, 120, and 150 s^{-1}. At each strain rate the frequency of the loudspeakers oscillation was varied and readings were taken at 25, 50, 100, and 200 Hz for constant amplitude. This was done for medium amplitude oscillation and an amplitude near the flow reversal amplitude. The speaker amplitude settings are shown in Table 5.1.

Because of feedback caused by the added enclosure, previously measured applied flow reversal voltages were no longer valid. The signal generator had to be at a much higher voltage setting to produce the same velocity oscillation, and because of the enclosure it was impossible to measure their exact values. This made it necessary to visually inspect the flame to estimate the amplitude. Measurements were taken as the flame seemed to be near the flow reversal amplitude and at roughly half the flow reversal amplitude. This methodology was kept consistent for each strain rate.

	Applied Speaker Voltage	
strain rate (s^{-1})	V/Vrev ~ 0.5	V/Vrev ~ 1.0
30	1	1.5
60	1	2.5
90	2	3
120	2.15	3.15
150	2.15	3.15

a)

	Applied Speaker Voltage	
strain rate (s^{-1})	V/Vrev ~ 0.5	V/Vrev ~ 1.0
30	1	1.5
60	1	1.5
90	2	3
120	2	3
150	2.15	4

b)

Table 5.1 – Applied Speaker Voltage for a) methane – air flame and b) propane – air flame.

5.1 Experimental Measurements for Methane CFDF

Figure 5.1.1 shows the NO concentration for CH_4 as a function of frequency and global steady strain rate for medium velocity oscillations (a) and near flow reversal oscillations (b). Both the medium and flow reversal amplitudes show a drop in NO

concentration between 25 and 100 Hz. This drop becomes much sharper as the amplitude reaches the flow reversal amplitude. For example, at GSR 90 s^{-1} the NO concentration drops from about 1 ppm at the medium amplitude and about 3 ppm at the near flow reversal amplitude. After the drop between 25 and 100 Hz the medium amplitude oscillation increases roughly 1 ppm between 100 and 200 Hz. However, for the strong velocity oscillation the NO concentration remains relatively constant between 100 and 200 Hz.

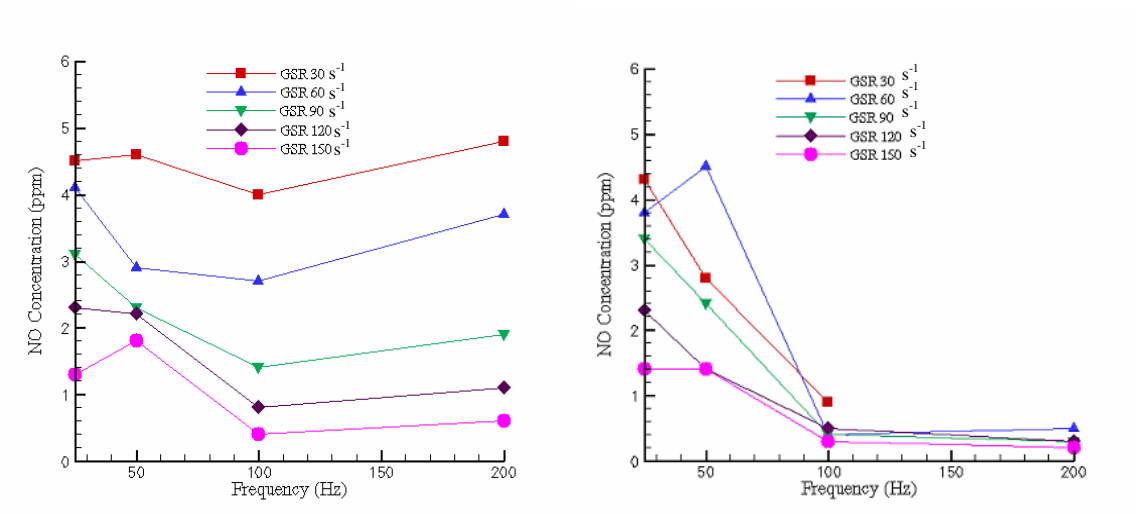

Figure 5.1.1 - NO concentration for methane – air flame as a function of frequency and global steady strain rate for medium velocity oscillations (a) and near flow reversal oscillations (b)

Figure 5.1.2a and b show the NO_x concentration for CH_4-air flame as a function of frequency and global steady strain rate. The trends for both the medium and near flow reversal amplitudes show a drop in NO_x concentration between 25 and 100 Hz. For the medium amplitude the drop is small between 25 and 50 Hz, but between 50 Hz and 100 Hz the drop is much steeper. This drop becomes much sharper as the amplitude reaches the flow reversal amplitude

After the drop between 25 and 100 Hz the medium amplitude oscillation increases the NO_x concentration roughly 1 ppm between 100 and 200 Hz. However, for the strong velocity oscillation the NO_x concentration drops about 1 ppm between 100 and 200 Hz. The flame extinguished before reaching the near flow reversal amplitude for GSR 30 s^{-1} and GSR 60 s^{-1}, which explains the increase on Figure 5.1.2b.

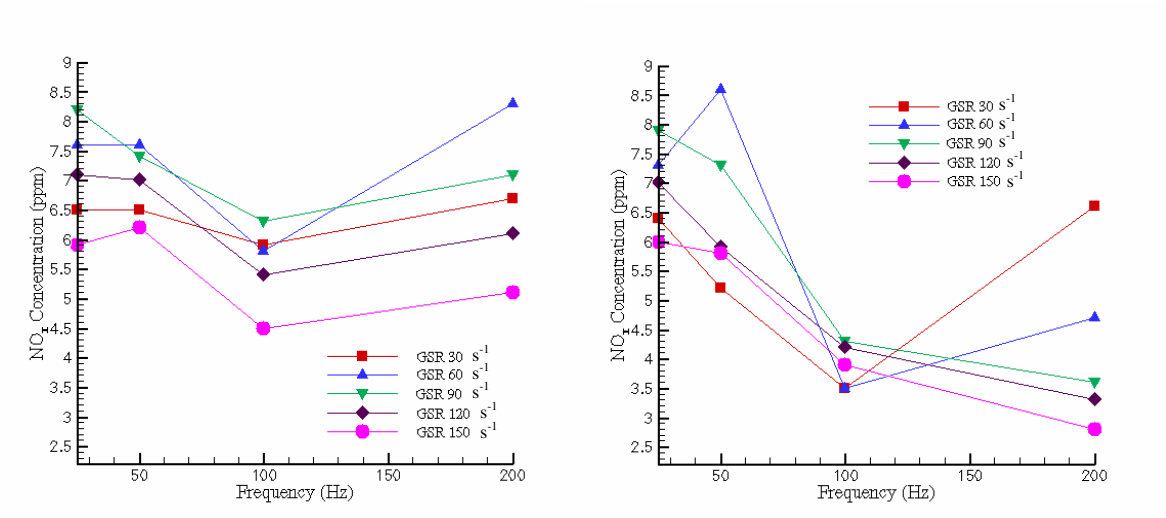

Figure 5.1.2 – NO_x concentration for methane – air flame as a function of frequency and global steady strain rate for medium velocity oscillations (a) and near flow reversal oscillations (b)

Figures 5.1.3 and 5.1.4 show how the NO and NO_x emission index, respectively, vary as a function of frequency, strain rate and forcing amplitude. These trends correspond very well with the concentration data. The main notable difference is how GSR 30 s^{-1} is very separated from the other strain rates. This is due to the increased nitrogen co-flow need to stabilize the flame at the low strain rate.

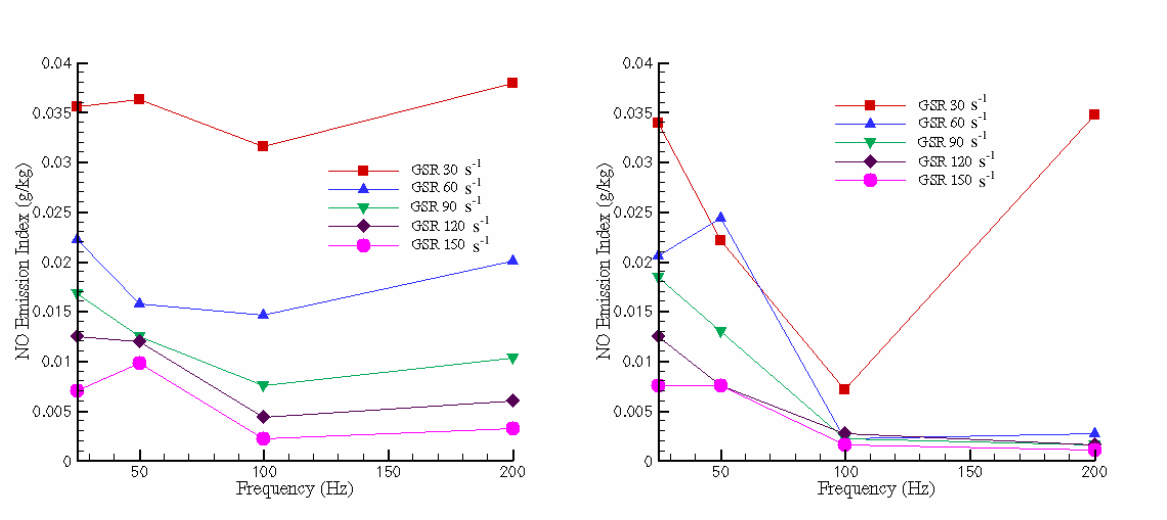

a) **b)**

Figure 5.1.3 – NO Emission Index for methane – air flame as a function of frequency and global steady strain rate for medium velocity oscillations (a) and near flow reversal oscillations (b)

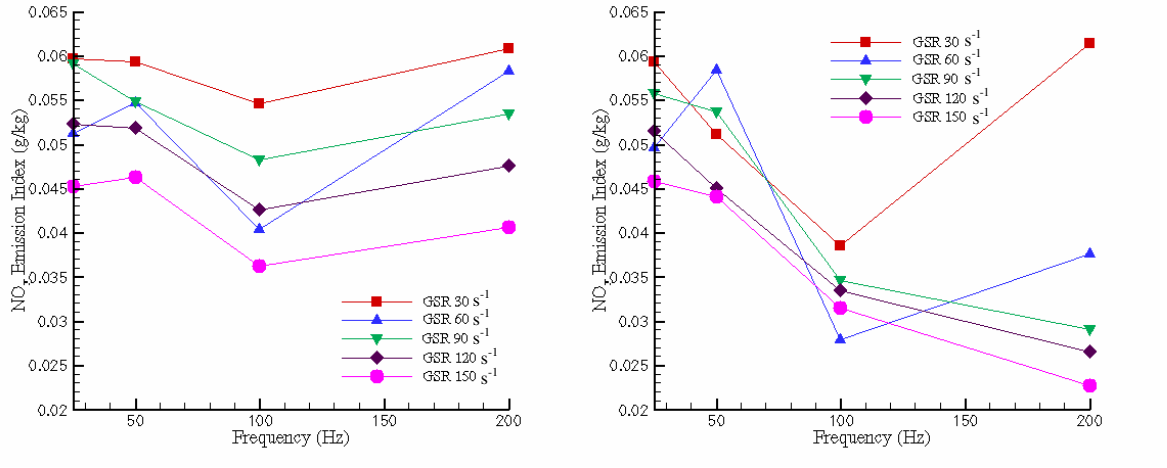

a) **b)**

Figure 5.1.4 – NO_x Emission Index for methane – air flame as a function of frequency and global steady strain rate for medium velocity oscillations (a) and near flow reversal oscillations (b)

5.2 Experimental Measurements for Propane CFDF's

Figure 5.2.1 shows the NO concentration for C_3H_8-air flame as a function of frequency and global steady strain rate for medium velocity oscillations (a) and near flow reversal oscillations (b). Both the medium and flow reversal amplitudes show a drop in NO concentration between 25 and 100 Hz at strain rates of 90, 120, and 150 Hz. As with

methane, this drop becomes much sharper as the amplitude approaches the flow reversal amplitude. However, at strain rates of 30 and 60 Hz the NO concentration is less sensitive to the oscillations for the medium forcing amplitude. Also, the 100 and 200 Hz measurements for 30 and 60 Hz in Figure 5.2.1b are unreliable because the flame extinguished before the correct amplitude could be reached.

After the drop between 25 and 100 Hz the medium amplitude oscillation increases the concentration roughly 2 ppm between 100 and 200 Hz for the higher strain rates. However, for the strong velocity oscillation the NO concentration only increases slightly between 100 and 200 Hz. This is more pronounced as the strain rate increases.

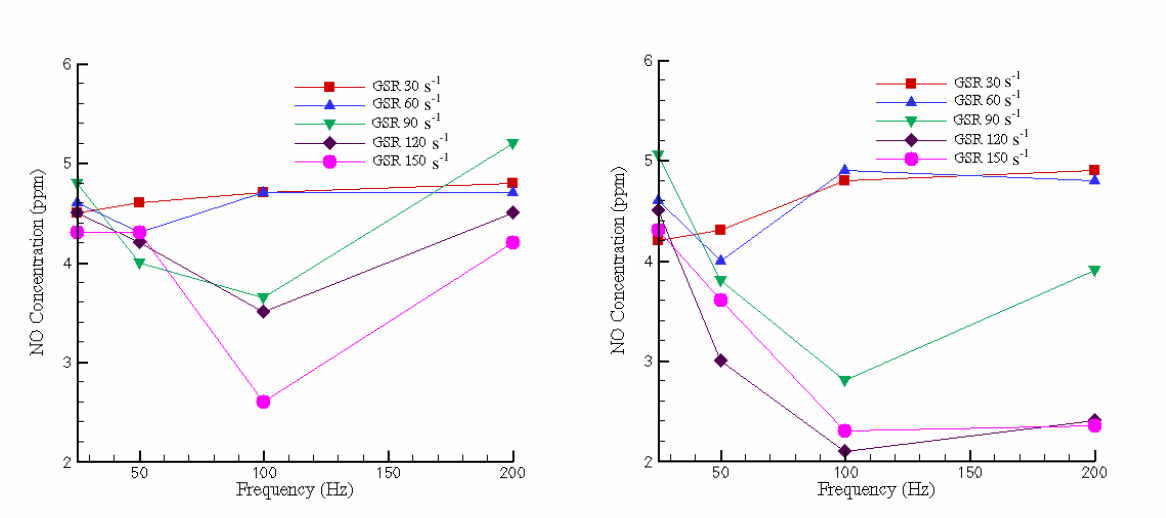

Figure 5.2.1 – NO concentrations for propane – air flame as a function of frequency and global steady strain rate for medium velocity oscillations (a) and near flow reversal oscillations (b).

Figure 5.2.2a and b show the NO_x concentration for C_3H_8 - air flames as a function of frequency and global steady strain rate. As with the NO concentration for propane-air flames, the NO_x concentration for both the medium and flow reversal amplitudes show a drop in concentration between 25 and 100 Hz for global strain rates of 90 s^{-1} and greater. This drop becomes more pronounced as the amplitude reaches the flow reversal amplitude.

After the drop between 25 and 100 Hz the medium amplitude oscillation increases the NO_x concentration roughly 1 ppm between 100 and 200 Hz for global strain rates of 90 and greater. However, for the strong velocity oscillation the NO_x concentration drops about 1 ppm between 100 and 200 Hz. As with the NO measurements the flame extinguished before reaching the flow reversal amplitude for GSR 30 and GSR 60.

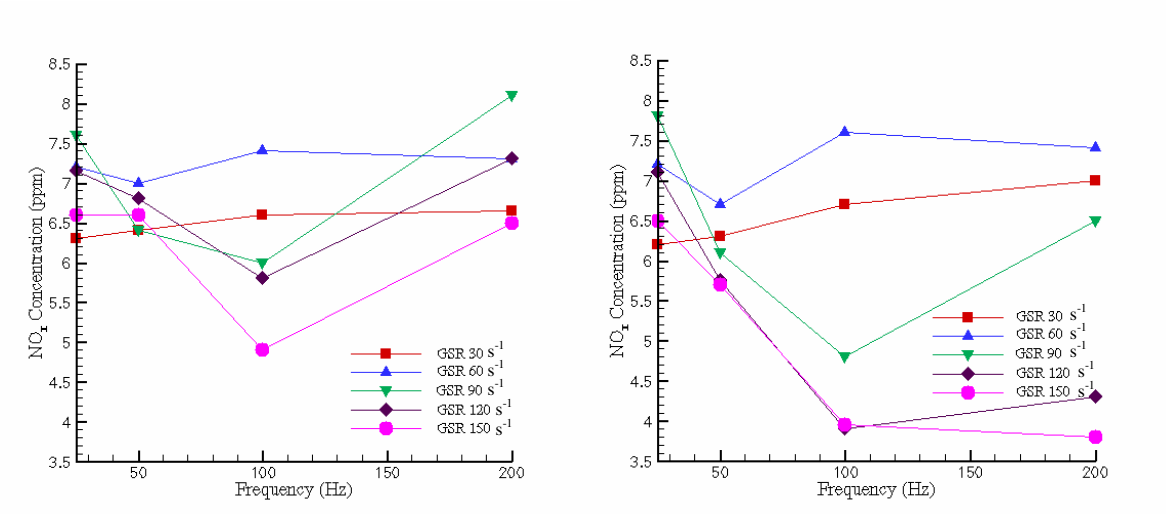

Figure 5.2.2 – NO_x concentrations for propane – air flame as a function of frequency and global steady strain rate for medium velocity oscillations (a) and near flow reversal oscillations (b).

Figures 5.2.3 and 5.2.4 show how the NO and NO_x emission index, respectively, vary as a function of frequency, strain rate and forcing amplitude. As with the methane emission index these trends correspond very well with the concentration data. Once again, the main notable difference is how GSR 30 s^{-1} is very separated from the other strain rates. This is due to the increased nitrogen co-flow need to stabilize the flame at the low strain rate.

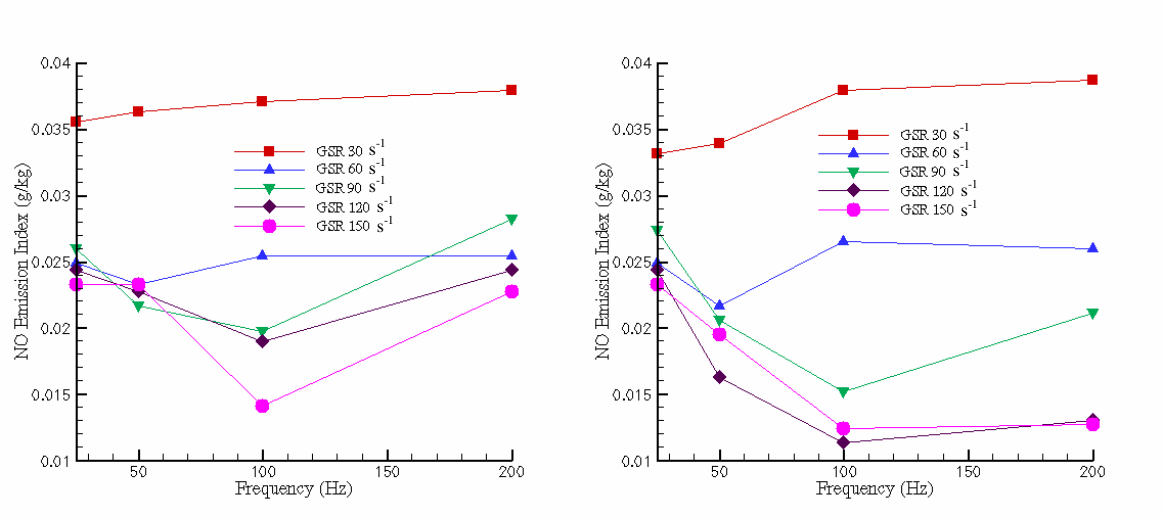

a) **b)**

Figure 5.2.3 – NO emission index for propane – air flame as a function of frequency and global steady strain rate for medium velocity oscillations (a) and near flow reversal oscillations (b).

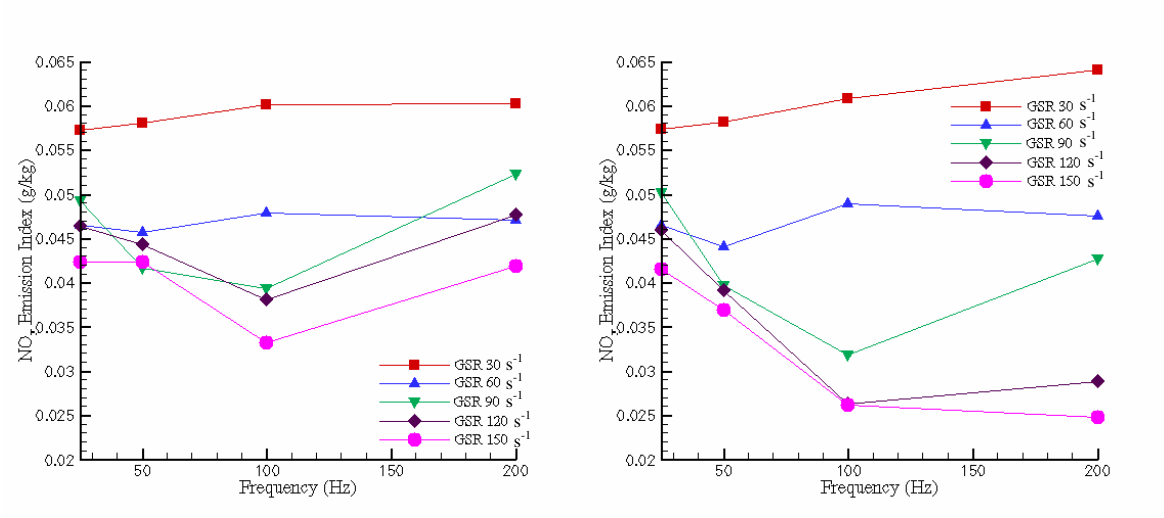

a) **b)**

Figure 5.2.4 – NO_x emission index for propane – air flame as a function of frequency and global steady strain rate for medium velocity oscillations (a) and near flow reversal oscillations (b).

5.3 Unsteady Computational Results for Methane CFDF's

Numerical calculations were done for methane – air flames subjected to unsteady strain rates using the opus code outlined in section 3. Computations were done for strain rates of 30, 60 and 90 s^{-1}. At each strain rate runs of 25, 50, 100 and 200 Hz were

calculated at forcing amplitudes of one half the flow reversal amplitude, and 95% of the flow reversal amplitude. The results were then compared to the experimental methane data. Propane was not calculated due to the lack of a reasonably sized propane mechanism.

Figure 5.3.1 shows how the phase of the peak flame temperature changes relative to the calculated strain rate for increasing frequency. At 25 and 50 Hz the flame responds quasi-steadily, because the temperature and strain rate are approximately 180 degrees out of phase. This makes sense because, for steady laminar diffusion flames, as the strain rate increases the temperature drops accordingly. However, as the frequency grows, the temperature begins to move into phase with the strain rate. This is goes along with the experimental findings of Welle (2002). Also, the NO mole fraction is directly in phase with the temperature, as shown in Figure 5.3.2. This is to be expected because of the nonlinear relationship between NO_x formation and temperature due to the Zel'dovich mechanism.

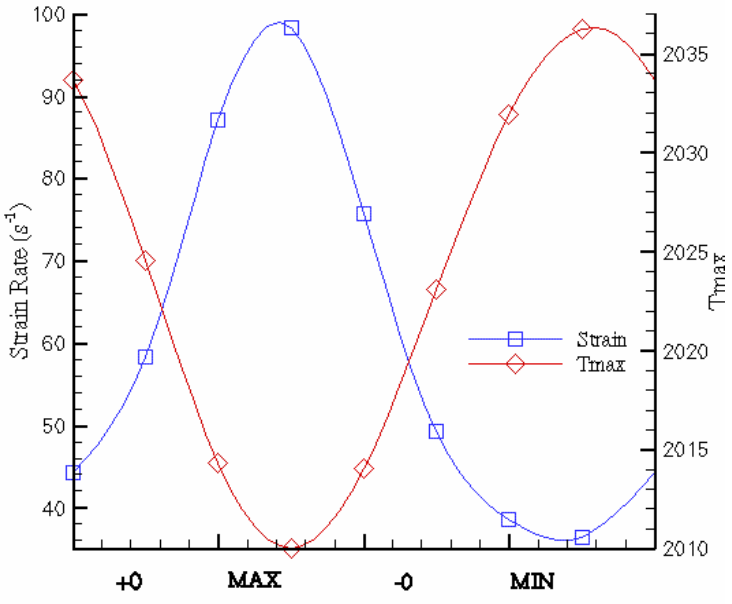

a)

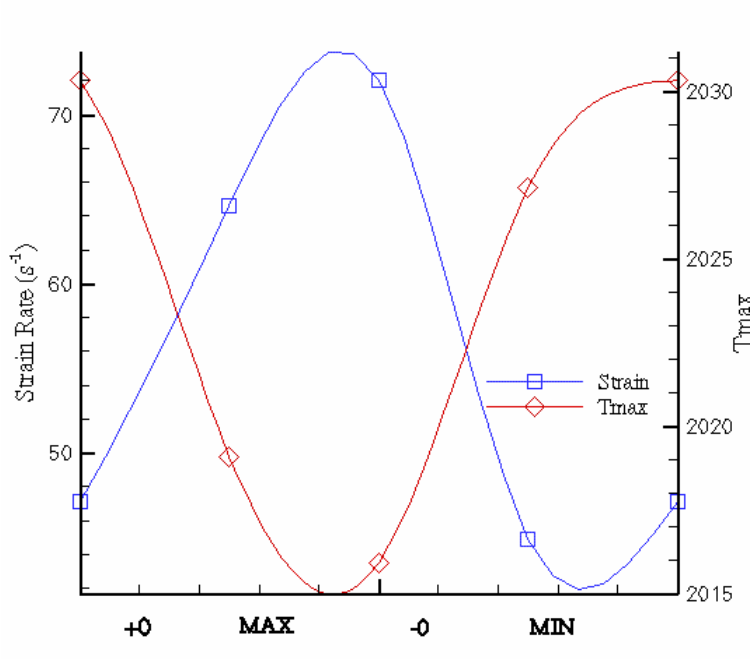

b)

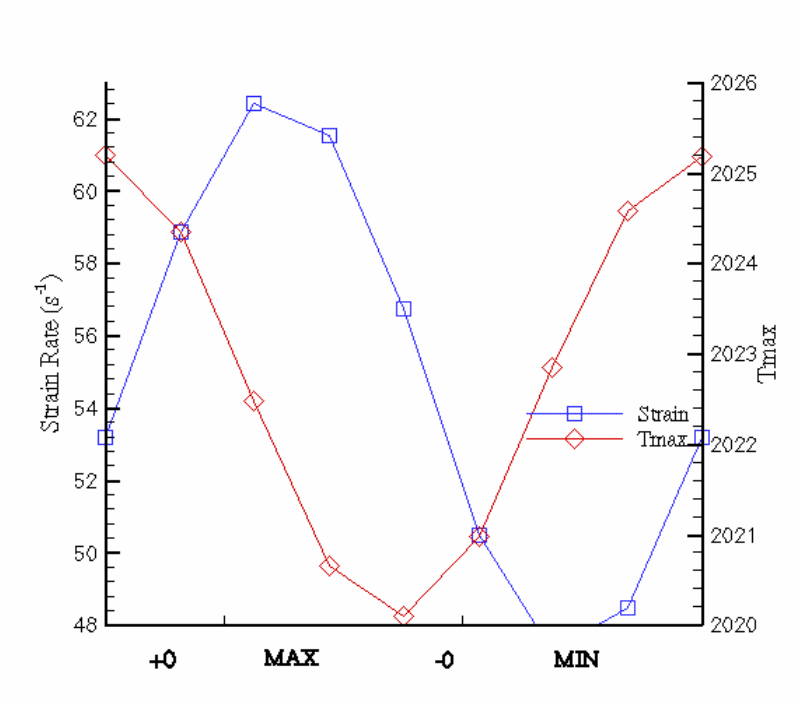

c)

Figure 5.3.1 – Phase relationship between the peak flame temperature and unsteady strain rate, a) 25 Hz, b) 50 Hz and c) 200 Hz.

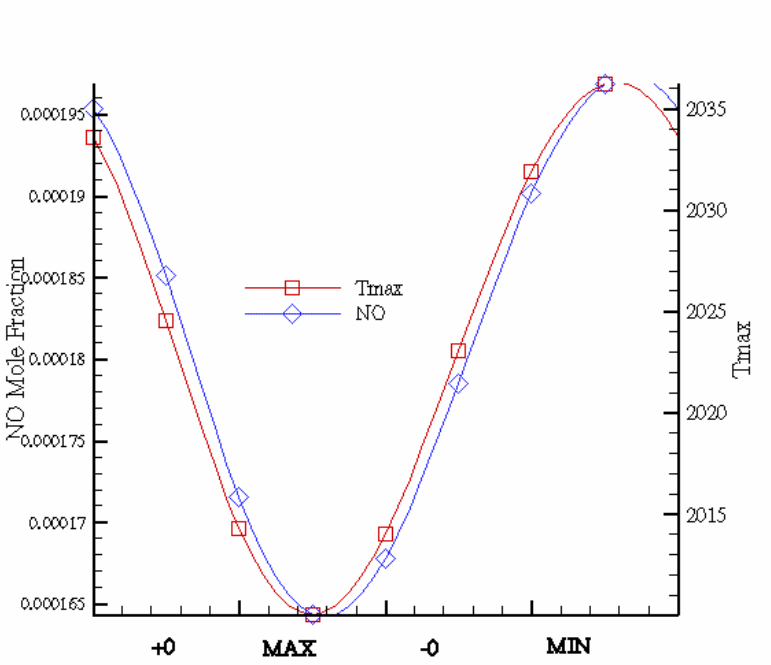

Figure 5.3.2 – Phase relationship between NO mole fraction and peak flame temperature at frequency of 200 Hz.

Figure 5.3.3 shows the variation of NO concentration as a function of global strain rate and frequency. The computational results show that at half of the flow reversal amplitude the NO concentration rises slightly above the calculated steady value, and drops slightly as the frequency increases. Between 50 and 100 Hz the concentration drops slightly below the steady value, and remains relatively constant with further increases in temperature. However, at 95 % of the flow reversal amplitude this effect is more pronounced. The concentration jumps roughly 1 ppm above the steady value. As with the medium amplitude, the high amplitude oscillation shows that the concentration drops below the steady value between 50 and 100 Hz. It then drops even lower than the medium amplitude, to roughly 1/3 ppm below the steady value. It is interesting to note how the large and medium amplitudes cross the steady value at the same frequency for each global strain rate. The computational NO_x concentration is show in Figure 5.3.4. As with the

steady computations the contribution of NO_2 to the total NO_x emission is very small, and follows the same pattern as the NO concentration.

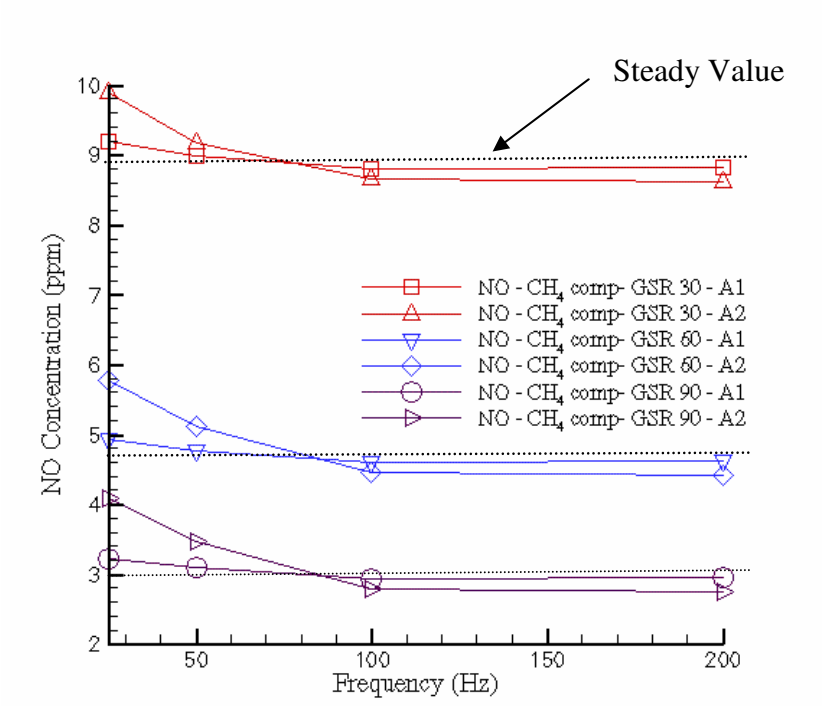

Figure 5.3.3 – Numerical NO concentration for methane – air flame as a function of forcing frequency, amplitude and strain rate.

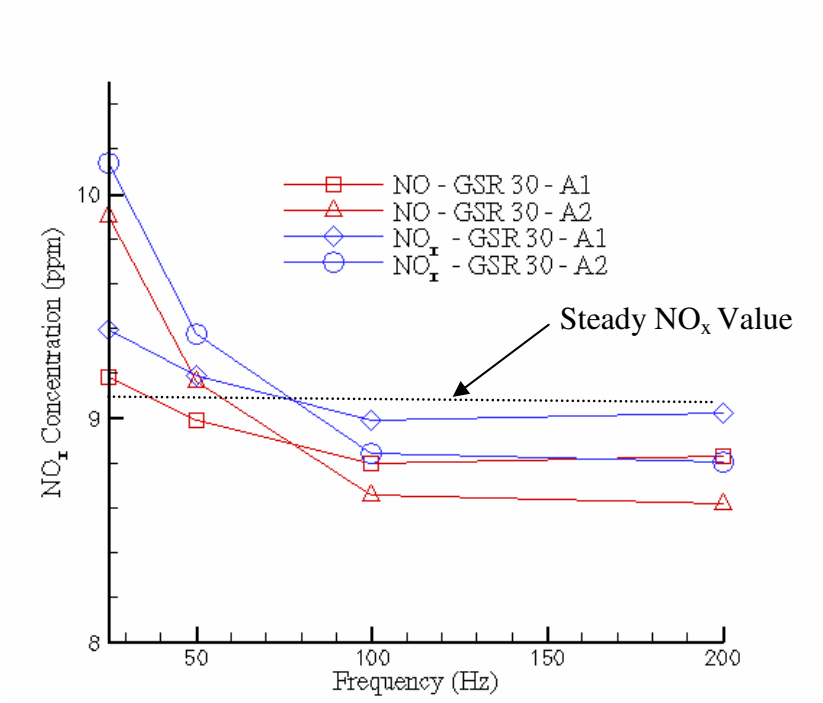

Figure 5.3.4 – Computational NO_x concentration as a function of frequency and amplitude for GSR 30 s^{-1}.

In order to better understand the experimental results it is important to directly compare the data to calculations. Figure 5.3.5a and b shows the experimental and computational NO concentrations for methane – air flames, plotted on the same graph for $U/U_{rev} = 0.5$ and $U/U_{rev} = 0.95$ respectively. At half of the flow reversal amplitude, aside from the already addressed difference at low strain rates, the experimental and computational trends match up reasonably well. Both measured and calculated NO concentration decreases as the frequency in increased up to about 100 Hz, and then increase up to 200 Hz. However, this is much more pronounced in the experimental data, whereas with the computational data it is much more subtle. A big difference between the two data sets is while the experimental data shows that the imposed oscillation causes the NO concentration to drop below the steady state value and then approach it again as the frequency is increased, a super-equilibrium condition seems to exist with the computational data. The imposed oscillation causes the NO concentration to rise above the steady value, and then approach it as the frequency is increased.

At 95% of the flow reversal amplitude the experimental data still drops below the steady value, however, the drop is much more significant. Also, after a frequency of 100 Hz the concentration no longer rises to the steady value, but rather decreases slightly. The exact same trends can be seen in the computational data, except that the initial frequencies are super-equilibrium and the drop to just below the steady value at approximately 90 Hz.

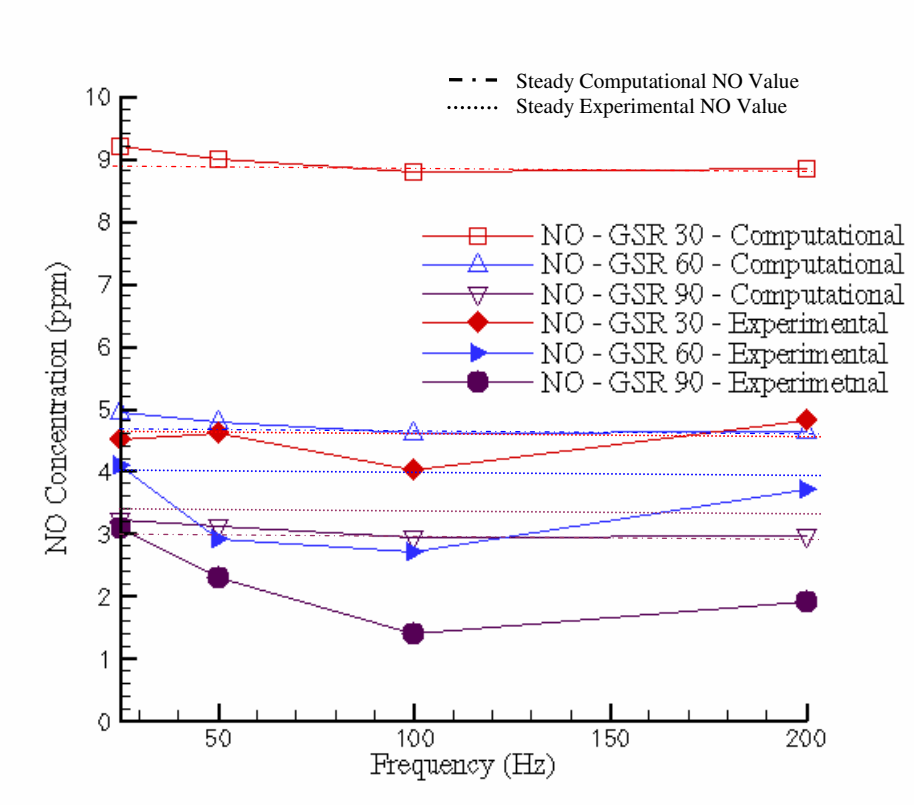

a)

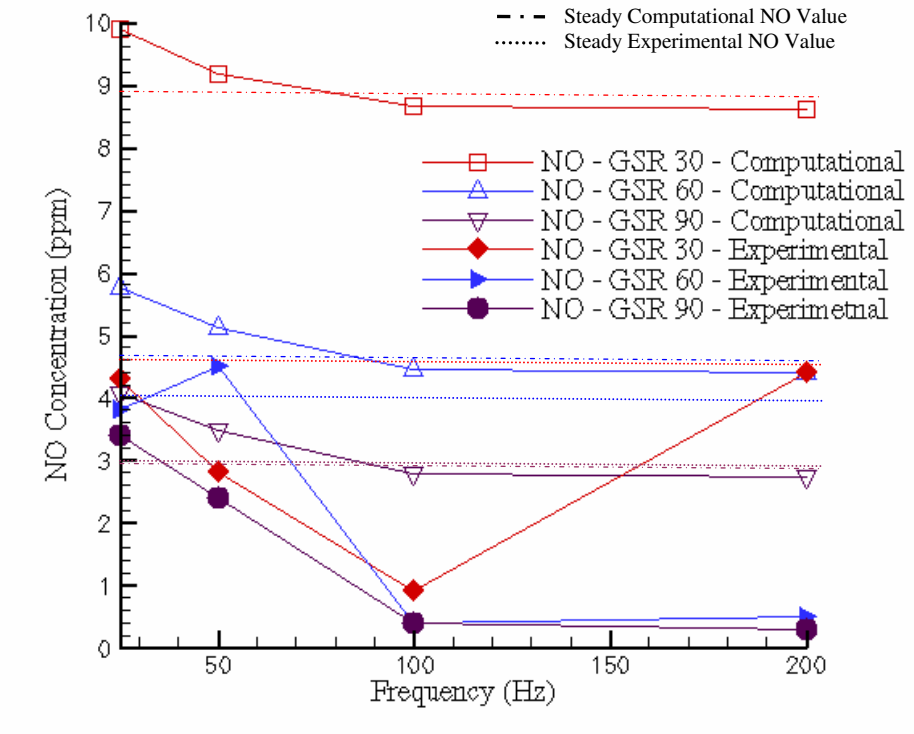

b)

Figure 5.3.5 - Experimental and computational NO concentrations for methane – air flames.

6 Conclusions

NO_x emissions are a very important consideration in combustor design. Not only are they very destructive to the natural environment, they are also hazardous to human health and wellbeing. While NO_x formation is fairly well understood in laminar diffusion and premixed flames for simple hydrocarbons, it is not well understood for turbulent diffusion flames or for more complex hydrocarbons. This is important because of the large number of practical combustion devices that incorporate turbulent diffusion flames. This research has focused on expanding the knowledge of NO_x formation in steady and unsteady counterflow diffusion flames. This research is also one of the first to computationally and experimentally study NO_x formation in unsteady counterflow diffusion flames. The conclusions that can be drawn from this research are as follows.

6.1 Steady Propane Counterflow Diffusion Flames

2. At high steady strain rates the NO concentration, for propane, decreases with increasing steady strain rate except at strain rates less than 60 s^{-1}. At strain rates less than 60 s^{-1} the opposite is true due to high soot loading, and thus, high radiative hear transfer.
3. The NO_x concentration increases with steady strain rate, which show that more NO_2 is produced at high strain rates. This is probably due to the fact that the high temperature zone of the flame is narrower at high strain rates.
4. The NO emission index drops very slightly with increasing steady strain rate, while the NO_x emission index drops slightly between 30 and 60 s^{-1} then begins to rise with increases of steady strain rate.

6.2 Steady Methane Counterflow Diffusion Flames

1. The NO concentration decreases with increasing steady strain rate, as expected.
2. The NO_x concentration shows a increase between 30 and 60 s^{-1} and then drops with further increases in steady strain rate.
3. The NO emission index drops slightly with increasing steady strain rate, while the NO_x emission index remains relatively constant with increasing steady strain rate. The experimental results matched the numerical results very well for NO at high strain rates. However at low strain rates, particularly 30 s^{-1}, experiment and computation diverge. At a strain rate of 30 s^{-1} computational results predict twice as much NO formation over what was experimentally measured. Even though methane is a low sooting fuel, soot is still present at the lower strain rates, causing some of the heat to be radiated away from the reaction zone. As the strain rate increases, the residence time of incipient soot particles in the high temperature zone is reduced and the total amount of soot decreases dramatically. According to computations and experiments conducted by Beltrame et al. (2001), higher concentration of soot in the flame leads to enhancement of radiant heat exchange, which acts to reduce temperature. This could account for the reduction in the NO concentration.
4. The OPPDIF code cannot model soot and PAH formation so the overall temperature is predicted to be higher, corresponding to a higher NO concentration. This becomes less predominant as the strain rate increases, because much less soot is created, hence why the experimental and computational data begin to converge.

5. Both EI_{NO} and EI_{NOx} for the computational data are considerably higher than their experimental counterparts. The slope of the EI_{NO} curve from the experimental data is much steeper than that of the predicted values. The substantial difference observed is most probably due to the very different methods used to calculate each.

6.3 Unsteady Propane Counterflow Diffusion Flames

1. Both the medium and flow reversal amplitudes show a drop in NO concentration between 25 and 100 Hz at strain rates of 90, 120, and 150 s^{-1}. This drop becomes much sharper as the amplitude reaches the flow reversal amplitude. However, at strain rates of 30 and 60 s^{-1} the NO concentration is less sensitive to the oscillations for the medium forcing amplitude.
2. Between 100 and 200 Hz the medium amplitude oscillation increases roughly 2 ppm for the higher strain rates. However, for the strong velocity oscillation the NO concentration only increases slightly between 100 and 200 Hz. This becomes more pronounced as the strain rate increases.
3. The NO_x concentrations follow the same trends as the NO concentration for propane – air unsteady counterflow diffusion flames
4. The emission index also follows the same trends as the NO concentration.

6.4 Unsteady Methane Counterflow Diffusion Flames

1. Both the medium and flow reversal amplitudes show a drop in NO concentration between 25 and 100 Hz. This drop becomes much sharper as the amplitude reaches the flow reversal amplitude. After the drop between 25 and 100 Hz the medium amplitude

oscillation increases slightly between 100 and 200 Hz. However, for the strong velocity oscillation the NO concentration remains relatively constant between 100 and 200 Hz.

2. The trends for both the medium and flow reversal amplitudes show a drop in NO_x concentration between 25 and 100 Hz. For the medium amplitude the drop is small between 25 and 50 Hz, but between 50 Hz and 100 Hz the drop is much steeper. This drop becomes much sharper as the amplitude reaches the flow reversal amplitude. After the drop between 25 and 100 Hz the medium amplitude oscillation increases the NO_x concentration slightly between 100 and 200 Hz. However, for the strong velocity oscillation the NO_x concentration drops slightly between 100 and 200 Hz.
3. The emission index trends correspond very well to the concentration data trends
4. The computations show that the temperature is initially 180 degrees out of phase with the strain rate, but as the frequency increases the temperature begins to move into phase with the strain rate. This matches well to previous experimental data.
5. The computed NO mole fraction is directly in phase with the temperature.
6. The experimental and computational trends match up reasonably well. Both measurements and calculations decrease as the frequency in increased up to about 100 Hz, and then increase up to 200 Hz. However, this is much more explicit in the experimental data, whereas with the computational data it is much more subtle. A big difference between the two data sets is while the experimental data shows that the imposed oscillation causes the NO concentration to drop below the steady state value and then approach it again as the frequency is increased, a super-equilibrium condition seems to exist with the computational data. The imposed oscillation causes the NO concentration to rise about the steady value, and then approach it as the frequency is

increased. At 95% of the flow reversal amplitude the experimental data still drops below the steady value, however, the drop is much more significant. Also, after a frequency of 100 Hz the concentration no longer rises to the steady value, it now decreases slightly. The exact same trends can be seen in the computational data, except that the initial frequencies are super-equilibrium and the drop to just below the steady value at approximately 90 Hz.

6.5 Future Work

Because of the considerably higher soot loading at the lower strain rates, which facilitates higher radiative heat transfer it would be beneficial to add both a soot model and a radiation model to the computational method.

12 References

Atreya, A., Zhang, C., Kim. H. K., Shamim, T. and Suh, J. (1996). "The Effect of Changes in the Flame Structure on the Formation and Destruction of Soot and NO_x in Radiating Diffusion Flames." *Twenty-Sixth Symposium (International) on Combustion*, The Combustion Institute, 2181-2189.

Axworthy, A. E. and Benson, S. W. (). "Mechanism of Gas Phase Decomposition of Ozone. Thermal and Photochemical Reactions." *Ozone Chemistry and Technology*, **21**: 388-397.

Barlow, R. S., Karpetis, A. N., Frank, J. H. and Chen, J. Y. (2001). "Scalar Profiles and NO Formation in Laminar Opposed-Flow Partially Premixed Methane/Air Flames." *Combustion and Flame*, **127:** 2102-2118.

Beltrame, A., Porshnev, P., Merchan-Merchan, W., Saveliev, A., Fridman, A., Kennedy, L. A., Petrova, O. Zhdanok, S., Amouri, F., and Charon, O. (2001) "Soot and NO Formation in Methane–Oxygen Enriched Diffusion Flames," *Combustion and Flame*, **124:** 295-310.

Blevins, L. G. and Gore, J. P. (1999). "Computed Structure of Low Strain Rate Partially Premixed CH_4/Air Counterflow Flames: Implication for NO Formation." *Combustion and Flame*, **116**: 546-566.

Bonturi, S. B., Pourkashanian, M., Williams, A., Oskam, G. and Wilson, C. (1996). "NO_x Formation in Counter-Flow Opposed-Jet Diffusion CH_4/Air Flames." *Combustion Science and Technology*, **121**: 217-233.

Bowman, C. T. (1992). "Control of Combustion-Generated Nitrogen Oxide Emissions: Technology Driven by Regulation." *Twenty-Fourth Symposium (International) on Combustion*, The Combustion Institute, 859-878.

Burke, SP and Schumann, T.E.W. (1928). "Diffusion Flames," *Combustion Symposium*, 76th Meeting of the Chemical Society, Swampscott, MA, 998-1003.

Caldeira-Pires, A., Heitor, M. V. and Carvalho, J. A. (2000). "Characteristics of Nitric Oxide Formation Rates in Turbulent Nonpremixed Jet Flames." *Combustion and Flame*, **120(3)**: 383-391.

Chao, Y. C., Huang, Y. W. and Wu, D. C. (2000). "Feasibility of Controlling NO_x Emissions from a Jet Flame by Acoustic Excitation." *Combustion Science and Technology*, **158**: 461-484.

Charlston-Goch, D., Chadwick, B.L., Morrison, R.J.S., Campisi, A., Thomsen, D.D., Laurendeau, N.M. (2001) "Laser-induced Fluorescence Measurements and Modeling of Nitric Oxide in Premixed Flames of CO+H-2+CH4 and Air at High Pressures I. Nitrogen Fixation," *Combustion and Flame*, **125:** 729-743.

Chen,S. L., Heap, M. P., Pershing, D. W. and Martin, G. B. (1982): *Fuel*, **61:** 1218.

DeBruhl, C. D., Roberts, W. L., and Echekki, T. (2003). "NO_x Measurements in an Unsteady Counterflow Diffusion Flame." *Proceedings of the Third Joint Meeting of the U.S. Sections of The Combustion Institute*, Chicago, IL.

DeCroix, M. E. (2003). Sandia National Labortories, private communication.

DeCroix, M. E., Roberts, W. L. and Gould, R. D. (1998). "Velocity Measurements in an Unsteady Counterflow Diffusion Flame Using Laser Doppler Velocimetry." *ASME Fluids Engineering Division Summer Meeting*, Washington, D.C., Paper 4920.

Dixon-Lewis, G., David, T., Gaskell, P. H., Fukutani, S., Jinno, H., Miller, J. A., Kee, R. J., Smooke, M. D., Peters, N., Effelsberg, E., Warnatz, J., Behrendt, F. (1984). "Calculation of the Structure and Extinction Limit of a Methane – Air Counterflow Diffusion Flame in the Forward Stagnation Region of a Porous Cylinder," *Twentieth Symposium (International) on Combustion,* The Combustion Institute, 1893-1904.

Drake, M. C. and Blint, R. J. (1989). "Thermal NO_x in Stretched Laminar Opposed-Flow Diffusion Flames with $CO/H_2/N_2$ Fuel." *Combustion and Flame*, **76**: 151-167.

Drake, M. C. and Blint, R. J. (1991). "Relative Importance of Nitric Oxide Formation Mechanisms in Laminar Opposed-flow Diffusion Flames." *Combustion and Flame*, **83**: 185-203.

Dupont, V. and Williams, A. (1998). "NO_x Mechanisms in Rich Methane – Air Flames," *Combustion and Flame*, **114:** 114-118.

Eberius, K. H. and Just, T. (1973). "Atmospheric Pollution by Jet Engines." *AGARD Conference Proceedings*, **AGARD-**CP-125, 16-1.

Echekki, T. (2003). North Carolina State University, private communication.

Egolfopoulos, F. N., (2000). "Structure and extinction of unsteady, counterflowing, strained, non-premixed flames," *INTERNATIONAL JOURNAL OF ENERGY RESEARCH* **24** (11): 989-1010.

Egolfopoulos, F. N. and Campbell, C. S. (1996). "Unsteady Counterflowing Strained Diffusion Flames: Diffusion Limited Frequency Response," *Journal of Fluid Mechanics,* **318**, 1.

Fenimore, C. P. (1971). "Formation of Nitric Oxide in Premixed Hydrocarbon Flames." *Thirteenth Symposium (International) on Combusiton*, The Combustion Institute, 373-389.

Ford, H. W., Doyle, G. J. and Endow, N. (1959). "Kinetics of Photolysis of Low Concentrations of Nitrogen Dioxide in Air." *Ozone Chemistry and Technology*, **21**: 410-415.

Frank, J. H., Barlow, R. S., Lundquist, C. and Pope, S. B. (2000). "Radiation and Nitric Oxide Formation in Turbulent Non-Premxied Jet Flames." *Proceeding of the Combustion Institute*, **28**: 447-454.

Fuse, R., Kobayashi, H., Ju, Y., Maruta, K. and Niioka, T. (2002). "NO_x Emission From High-Temperature Air/Methane Counterflow Diffusion Flame." *International Journal of Thermal Sciences*, **41**: 693-698.

Glarborg, P., Miller, J. A., Kee, R. J. (1986) "Kinetic Modeling and Sensitivity Analysis of Nitrogen Oxide Formation in Well-Stirred Reactors," *Combustion and Flame,* **65(2)**: 177-202.

Glassman, I. (1996). *Combustion (Third Edition)*, Academic Press.

Grcar, J.F. (1992). "The Twopnt Program for Boundary Value Problems," Sandia National Laboratories Report SAND91-8230.

Hahn, W. A. and Wendt, J. O. L. (1981). "NO_x Formation in Flat, Laminar, Opposed Jet Methane Diffusion Flames." *Eighteenth Symposium (International) on Combustion*, The Combustion Institute, 121-131.

Hayhurst, A. N. and Vince, I. M. (1983). "The Origin and Nature of "Prompt" Nitric Oxide in Flames." *Combustion and Flame*, **50**: 41-57.

Im, H. G., Law, C. K., Kim, J. S. and Williams, F. A. (1995). "Response of Counterflow Diffusion Flames to Oscillation Strain Rates." *Combustion and Flame*, **100**: 21-30.

Im, H. G., Chen, J. H., and Chen, J. Y. (1999). "Chemical Response of Methane/Air diffusion Flames to Unsteady Strain Rate." *Combustion and Flame*, **118**: 204-212.

Im, H. G., Raja, L. L., Kee, R. J., Lutz, A. E., and Petzold, L. R. (2000). OPUS: A Fortran Program for Unsteady Opposed-Flowed Flames, Sandia National Laboratories Report SAND2000-8211. July 2000.

Johnston, H. and Whitten, G. (1973). "Reaction of Ozone with Nitrogen Oxides at High Altitudes." *AGARD Conference Proceedings*. **AGARD-CP**-125, 2-1.

Johnsson, J. E., Glarborg, P. and Dam-Johansen, K. (1992). "Thermal Dissociation of Nitrous Oxide at Medium Temperatures." *Twenty-Fourth Symposium (International) on Combustion*, The Combustion Institute, 917-924.

Kee, R. J., Dixon-Lewis, G., Warnatz, J., Coltrin, M. E., and Miller, J. A. (1986). "A Fortran Computer Code Package for the Evaluation of Gas-Phase Multicomponent Transport Properties," Sandia National Laboratories Report SAND86-8246.

Kee. R. J., Rupley, F. M. and Miller, J. A. (1991). Chemkin-II: A Fortran Chemical Kinetics Package for the Analysis of Gas-Phase Chemical Kinetics, Sandia National Laboratories Report SAND89-8009B. November 1991.

Konnov, A.A., Dyakov, I.V., De Ruyck, J. (2003) "Nitric Oxide Formation in Premixed Flames of H-2+CO+CO2 and Air," *Proceeding of the Combustion Institute*, **29:** 2171-2177 Part 2.

Kuo, K. K. (1986) *Principles of Combusiton*, Wiley-Interscience.

Lee, C. E., Lee, S. R., Han, J. W., and Park, J. (2001). "Numerical Study on Effect of CO_2 Addition in Flame Structure and NO_x Formation of CH_4-air Counterflow diffusion Flames." *International Journal of Energy Research*, **25**: 343-354.

Lilleheie, N. I., Byggstøyl, S., Magnussen, B. F., Kilpinen, P. and Hupa, M. (1992)."A Reduced Mechanism for Nitrogen Chemistry in Methane Combustion." *Twenty-Fourth Symposium (International) on Combustion*, The Combustion Institute, 889-898.

Lutz, A. E., Kee, R. J., Grcar, J. F., and Rupley, F. M. (1996). OPPDIF: A Fortran Program For Computing Opposed-Flow Diffusion Flames. Sandia National Laboratories Report, SAND96-8243. May 1996.

Meunier, P., Costa, M. and Carvalho, M. G. (1998). "On NO_x Emissions from Turbulent Propane Diffusion Flames." *Combustion and Flame*, **112(1-2)**: 221-230.

Miller, J. A. and Bowman, C. T. (1989). "Mechanism and Modeling of Nitrogen Chemistry in Combustion." *Progress in Energy and Combustion Science*, **15**: 287-338.

Naik, S. V. and Laurendeau, N. M. (2002). "Quantitative Laser-Saturated Fluorescence Measurements of Nitric Oxide in Counter-Flow Diffusion Flames under Sooting Oxy-Fuel Conditions." *Combustion and Flame*, **129**: 112-119.

Nishioka, M., Nakagawa, S., Ishikawa, Y., and Takeno, T. (1994). "NO Emission Characteristics of Methane - Air Double Flames," *Combustion and Flame*, **98**: 127-138.

Peters, N., (1984) "Laminar Diffusion Flamelet Models in Non-Premixed Turbulent
Combustion", *Progress in Energy and Combustion Science*, **10**, 319-339.

Peters, N. (1986) "Laminar Flamelet Concepts in Turbulent Combustion", *Proceedings of the Combustion Institute*, **21**, 1231-1250.

Peters, N., "Turbulent Combustion", Cambridge Press, pp. 184 (2000).

Pitsch, H., Chen, M., Peters, N., (1998) "Unsteady Flamelet Modeling of Turbulent Hydrogen-air Diffusion Flames", *Proceedings of the Combustion Institute*, **27**, 1057-1064.

Riggen-DeCroix, M. E. (1998). "The Effects of Unsteady Hydrodynamics on Soot Formation in a Counterflow Diffusion Flame." Ph.D. Thesis, North Carolina State University.

Ravikrishna, R. V., Cooper, C. S. and Laurendeau, N. M. (1999). "Comparison of Saturated and Linear Laser-Induced Fluorescence Measurements of Nitric Oxide in Counterflow Diffusion Flames." *Combustion and Flame*, **117**: 810-820.

Ravikrishna, R. V., Douglas, D. and Laurendeau, N. M. (2000). "Laser-Induce Fluorescence Measurements and Modeling of Nitric Oxide in High-Pressure Counterflow Diffusion Flames." *Combustion Science and Technology*, **157**: 243-261.

Ravikrishna, R. V. and Laurendeau, N. M. (1998). "Laser-saturated Fluorescence Measurements of Nitric Oxide in Laminar Counterflow Diffusion Flames." *Combustion and Flame*, **113**: 473-475.

Ravikrishna, R. V. and Laurendeau, N. M. (1999). "Laser-Induce Fluorescence Measurements and Modeling of Nitric Oxide in Methane-Air and Ethane-Air Counterflow Diffusion Flames." *Combustion and Flame*, **120**: 372-382.

Ravikrishna, R. V. and Laurendeau, N. M. (2000). "Laser-Induced Fluorescence Measurements and Modeling of Nitric Oxide in Counterflow Partially Premixed Flames." *Combustion and Flame*, **122**: 474-482.

Rørtveit, G. J., Hustad, J. E., Li., S. C., and Williams, F. A. (2002). "Effects of Diluents on NO_x Formation in Hydrogen Counterflow Flames." *Combustion and Flame*, **130**: 48-61.

Sanders, J. P. H., Chen, J. –Y., and Gokalp, I. (1997) "Flamelet-Based Modeling of NO Formation in Turbulent Hydrogen Jet Diffusion Flames," *Combustion and Flame*, **111:** 1-15.

Santoianni, D. A. (1999). "Temperature Imaging in Unsteady Propane-Air Counterflow Diffusion Flames Using Planar Laser-Induced Fluorescence of OH." Masters Thesis, North Carolina State University.

Seshadri, K., and Peters, N. (1988). "Asymptotic Structure and Extinction of Methane – Air Diffusion Flames," *Combustion and Flame*, **73**.

Seshadri, K., and Williams, F. A. (1978), *International Journal of Heat and Mass Transfer,* **21:**251.
Smyth, K. C., (1996). "NO Production and Destruction in a Methane/Air Diffusion Flame," *Combustion Science and Technology*, **115(1-3):** 151-176.

Sohn, C. H., Jeong, I. M. and Chung, S. H. (2002). "Numerical Study of the Effects of Pressure and Air-Dilution on NO Formation in Laminar Counterflow Diffusion Flames of Methane in High Temperature Air." *Combustion and Flame*, **130**: 83-93.

Song, Y. H., Bartok, W., Blair, D. W. and Siminski, V. J. (1981*): Eighteenth Symposium (International) on Combustion,* The Combustion Institute, 53.

Spalding, D.B. (1961). "Theory of Mixing and Chemical Reaction in the Opposed-Jet Diffusion Flame," *ARS J.*, **31**, 763-771.

Sung, C. J., Liu, J. B. and Law, C. K. (1995). "Structural Response of Counterflow Diffusion Flames to Strain Rate Variations." *Combustion and Flame*, **102**: 481-492.

Takeno, T. and Nishioka, M. (1993). "Species Conservation and Emission Indices for Flames Described by Similarity Solutions." *Combustion and Flame*, **92**: 465-468.

Thomsen, D. D. and Laurendeau, N. M. (2001). "LIF Measurements and Modeling of Nitric Oxide Concentration in Atmospheric Counterflow Premixed Flames." *Combustion and Flame*, **124**: 350-369.

Tsuji, H. (1982). "Counterflow Diffusion Flames," *Progress in Energy and Combustion Sciences,* **8**, 93-119.

Turns, S. R. and Myhr, F. H. (1991). "Oxides of Nitrogen Emissions from Turbulent Jet Flames: Part I – Fuel Effects and Flame Radiation." *Combustion and Flame*, **87**: 319-335.

Turns, S. R. (1995). "Understanding NO_x Formation in Nonpremixed Flames: Experiments and Modeling." *Progress in Energy and Combustion Sciences*, **21**: 361-385.

Wang, J. and Niioka, T. (2001). "The Effect of Radiation Reabsorption on NO Formation in CH_4/air Counterflow Diffusion Flames." *Combustion Theory Modeling*, **5**: 385-398.

Welle, E. J. (2002). "The Frequency Response of Counterflow Diffusion Flames." Ph.D. Thesis, North Carolina State University.

Yamashita, H., Nishioka, M. and Takeno, T. (1997). "Prediction of NO_x Production Rate in Turbulent Diffusion Flames," *Energy Conservation Management,* **38(10-13):** 1343-1352.

Zel'dovich, J., (1946). *Acta physicochimica URSS,* **21:** 577.

8 APPENDICES

8.1 Flow Meter Settings

8.1.1 Global Strain Rate Conditions for Methane Counterflow Diffusion Flames.

Strain Rate (s^{-1})	V air (cm/s)	V fuel (cm/s)	Qair (slpm)	Q fuel (slpm)	V nitrogen (cm/s)	Q nitrogen (slpm)
30	18.96	25.25	5.20	6.92	18.96	7.86
60	38.29	50.99	10.50	13.98	38.29	15.88
90	57.26	76.23	15.70	20.90	57.26	23.74
120	76.22	101.48	20.90	27.83	76.22	31.60
150	95.19	126.73	26.10	34.75	95.19	39.46

8.1.2 Global Strain Rate Conditions for Methane Counterflow Diffusion Flames.

Strain Rate (s^{-1})	V air (cm/s)	V fuel (cm/s)	Qair (slpm)	Q fuel (slpm)	V nitrogen (cm/s)	Q nitrogen (slpm)
30	18.96	15.08	5.20	4.14	18.96	7.86
60	38.29	30.45	10.50	8.35	38.29	15.88
90	57.26	45.53	15.70	12.49	57.26	23.74
120	76.22	60.62	20.90	16.62	76.22	31.60
150	95.19	75.70	26.10	20.76	95.19	39.46

8.2 NO Profile Integration Code

```
**********************************************************************
h=1
 do J=1,JJ-1
        CALL CKYTX (S(NY,J), IWORK, RWORK, XMF)
        CALL CKRHOY (P+S(NP,J), S(NT,J), S(NY,J), IWORK, RWORK, RHO)
       dx(h)=X(J+1)-X(J)
       h=h+1
          write(*,*)'test',dx(h-1),h
     end do
     h=1
     do J=1,JJ-1
       CALL CKYTX (S(NY,J), IWORK, RWORK, XMF)
       CALL CKRHOY (P+S(NP,J), S(NT,J), S(NY,J), IWORK, RWORK, RHO)

          CALL CKYTX (S(NY,J+1), IWORK, RWORK, XMFp1)
       CALL CKRHOY (P+S(NP,J+1), S(NT,J+1), S(NY,J+1), IWORK,
    1              RWORK, RHO)

          ppmnot=(1./2.)*(XMF(KW(2))/S(NT,J)+XMFp1(KW(2))/S(NT,J+1))*
    1        dx(h)
          ppmno2t=(1./2.)*(XMF(KW(3))/S(NT,J)+XMFp1(KW(3))/S(NT,J+1))*
    1        dx(h)
          tempt = (1./2.)*(1./S(NT,J)+1./S(NT,J+1))*dx(h)


         ppmno = ppmnot+ppmno
            ppmno2 = ppmno2+ppmno2t
         temp = temp +tempt
            write(*,*)J,ppmnot,ppmno2t,tempt,ppmno,ppmno2,temp
          h=h+1
          end do
          molefracno=(ppmno/temp)*10**6.
          molefracno2=(ppmno2/temp)*10**6.
       WRITE (LPPOUT, *) TIME,molefracno,molefracno2
**********************************************************************
```

8.3 Velocity Boundary Condition Function

```
C*****************************************************************
C     BOUNDARY FUNCTIONS
C=================================================================
      DOUBLE PRECISION FUNCTION F0_VBC(T,AMP,FRE,T0)

C*****Boundary function for Velocity at X = 0

      IMPLICIT DOUBLE PRECISION (A-H, O-Z), INTEGER (I-N)

      DATA PI/3.14159265358973/
      PI2=2.*PI

      F0_VBC=(1.+AMP*(((exp(2.*(T)**3.)-1.)/(exp(2.*(T)**3.)+1.))
     1       )**0.5*(SIN(PI2*FRE*T)))

      RETURN
      END

      DOUBLE PRECISION FUNCTION F0_DVDTBC(T,AMP,FRE,T0)

C*****Boundary function for dV/dt Velocity at X = 0

      IMPLICIT DOUBLE PRECISION (A-H, O-Z), INTEGER (I-N)

      DATA PI/3.14159265358973/
      PI2=2.*PI

      F0_DVDTBC =(AMP*((exp(2*T**3.)-1)/(exp(2*T**3.)+1))**0.5*0.5*
     1          (2*T**3.*3./T*exp(2*T**3.)/(exp(2*T**3.)+1)-2*
     2          (exp(2*T**3.)-1)/(exp(2*T**3.)+1)**2*T**3.*3./T*
     3          exp(2*T**3.))/(exp(2*T**3.)-1)*(exp(2*T**3.)+1)*
     4          SIN(PI2*FRE*T)+AMP*((exp(2*T**3.)-1)/
     5          (exp(2*T**3.)+1))**0.5*COS(PI2*FRE*T)*PI2*FRE)

      RETURN
      END
C=================================================================
      DOUBLE PRECISION FUNCTION FL_VBC(T,AMP,FRE,T0)

C*****Boundary function for Velocity at X = L

      IMPLICIT DOUBLE PRECISION (A-H, O-Z), INTEGER (I-N)

      DATA PI/3.14159265358973/
```

```
      PI2=2.*PI

      FL_VBC=(1.+AMP*(((exp(2.*(T)**3.)-1.)/(exp(2.*(T)**3.)+1.)))
     1       **0.5*(SIN(PI2*FRE*T)))

      RETURN
      END

      DOUBLE PRECISION FUNCTION FL_DVDTBC(T,AMP,FRE,T0)

C*****Boundary function for Velocity at X = L

      IMPLICIT DOUBLE PRECISION (A-H, O-Z), INTEGER (I-N)

      DATA PI/3.14159265358973/
      PI2=2.*PI

      FL_DVDTBC =(AMP*((exp(2*T**3.)-1)/(exp(2*T**3.)+1))**0.5*0.5*
     1         (2*T**3.*3./T*exp(2*T**3.)/(exp(2*T**3.)+1)-2*
     2         (exp(2*T**3.)-1)/(exp(2*T**3.)+1)**2*T**3.*3./T*
     3         exp(2*T**3.))/(exp(2*T**3.)-1)*(exp(2*T**3.)+1)*
     4         SIN(PI2*FRE*T)+AMP*((exp(2*T**3.)-1)/
     5         (exp(2*T**3.)+1))**0.5*COS(PI2*FRE*T)*PI2*FRE)

      RETURN
      END
```

8.4 Elements and Species Considered in Reaction Mechanism

ELEMENTS

O H C N AR

END

SPECIES

H_2	H	O	O_2	OH	H_2O	HO_2	H_2O_2
C	CH	CH_2	$CH_2(S)$	CH_3	CH_4	CO	CO_2
HCO	CH_2O	CH_2OH	CH_3O	CH_3OH	C_2H	C_2H_2	C_2H_3
C_2H_4	C_2H_5	C_2H_6	HCCO	CH_2CO	HCCOH	N	NH
NH_2	NH_3	NNH	NO	NO_2	N_2O	HNO	CN
HCN	H_2CN	HCNN	HCNO	HOCN	HNCO	NCO	N_2
AR	C_3H_7	C_3H_8	CH_2CHO	CH_3CHO			

END

8.5 GRI Reaction Mechanism

```
REACTIONS
2O+M<=>O2+M                               1.200E+17   -1.000        .00
H2/ 2.40/ H2O/15.40/ CH4/ 2.00/ CO/ 1.75/ CO2/ 3.60/ C2H6/ 3.00/ AR/  .83/
O+H+M<=>OH+M                              5.000E+17   -1.000        .00
H2/2.00/ H2O/6.00/ CH4/2.00/ CO/1.50/ CO2/2.00/ C2H6/3.00/ AR/ .70/
O+H2<=>H+OH                               3.870E+04    2.700    6260.00
O+HO2<=>OH+O2                             2.000E+13     .000        .00
O+H2O2<=>OH+HO2                           9.630E+06    2.000    4000.00
O+CH<=>H+CO                               5.700E+13     .000        .00
O+CH2<=>H+HCO                             8.000E+13     .000        .00
O+CH2(S)<=>H2+CO                          1.500E+13     .000        .00
O+CH2(S)<=>H+HCO                          1.500E+13     .000        .00
O+CH3<=>H+CH2O                            5.060E+13     .000        .00
O+CH4<=>OH+CH3                            1.020E+09    1.500    8600.00
O+CO(+M)<=>CO2(+M)                        1.800E+10     .000    2385.00
   LOW/ 6.020E+14     .000    3000.00/
H2/2.00/ O2/6.00/ H2O/6.00/ CH4/2.00/ CO/1.50/ CO2/3.50/ C2H6/3.00/ AR/ .50/
O+HCO<=>OH+CO                             3.000E+13     .000        .00
O+HCO<=>H+CO2                             3.000E+13     .000        .00
O+CH2O<=>OH+HCO                           3.900E+13     .000    3540.00
O+CH2OH<=>OH+CH2O                         1.000E+13     .000        .00
O+CH3O<=>OH+CH2O                          1.000E+13     .000        .00
O+CH3OH<=>OH+CH2OH                        3.880E+05    2.500    3100.00
O+CH3OH<=>OH+CH3O                         1.300E+05    2.500    5000.00
O+C2H<=>CH+CO                             5.000E+13     .000        .00
O+C2H2<=>H+HCCO                           1.350E+07    2.000    1900.00
O+C2H2<=>OH+C2H                           4.600E+19   -1.410   28950.00
O+C2H2<=>CO+CH2                           6.940E+06    2.000    1900.00
O+C2H3<=>H+CH2CO                          3.000E+13     .000        .00
O+C2H4<=>CH3+HCO                          1.250E+07    1.830     220.00
O+C2H5<=>CH3+CH2O                         2.240E+13     .000        .00
O+C2H6<=>OH+C2H5                          8.980E+07    1.920    5690.00
O+HCCO<=>H+2CO                            1.000E+14     .000        .00
O+CH2CO<=>OH+HCCO                         1.000E+13     .000    8000.00
O+CH2CO<=>CH2+CO2                         1.750E+12     .000    1350.00
O2+CO<=>O+CO2                             2.500E+12     .000   47800.00
O2+CH2O<=>HO2+HCO                         1.000E+14     .000   40000.00
H+O2+M<=>HO2+M                            2.800E+18    -.860        .00
O2/ .00/ H2O/ .00/ CO/ .75/ CO2/1.50/ C2H6/1.50/ N2/ .00/ AR/ .00/
H+2O2<=>HO2+O2                            2.080E+19   -1.240        .00
H+O2+H2O<=>HO2+H2O                        11.26E+18    -.760        .00
H+O2+N2<=>HO2+N2                          2.600E+19   -1.240        .00
H+O2+AR<=>HO2+AR                          7.000E+17    -.800        .00
H+O2<=>O+OH                               2.650E+16    -.6707  17041.00
2H+M<=>H2+M                               1.000E+18   -1.000        .00
H2/ .00/ H2O/ .00/ CH4/2.00/ CO2/ .00/ C2H6/3.00/ AR/ .63/
2H+H2<=>2H2                               9.000E+16    -.600        .00
2H+H2O<=>H2+H2O                           6.000E+19   -1.250        .00
2H+CO2<=>H2+CO2                           5.500E+20   -2.000        .00
H+OH+M<=>H2O+M                            2.200E+22   -2.000        .00
H2/ .73/ H2O/3.65/ CH4/2.00/ C2H6/3.00/ AR/ .38/
H+HO2<=>O+H2O                             3.970E+12     .000     671.00
H+HO2<=>O2+H2                             4.480E+13     .000    1068.00
H+HO2<=>2OH                               0.840E+14     .000     635.00
H+H2O2<=>HO2+H2                           1.210E+07    2.000    5200.00
H+H2O2<=>OH+H2O                           1.000E+13     .000    3600.00
H+CH<=>C+H2                               1.650E+14     .000        .00
H+CH2(+M)<=>CH3(+M)                       6.000E+14     .000        .00
     LOW  /  1.040E+26   -2.760   1600.00/
     TROE/   .5620  91.00  5836.00  8552.00/
H2/2.00/ H2O/6.00/ CH4/2.00/ CO/1.50/ CO2/2.00/ C2H6/3.00/ AR/ .70/
H+CH2(S)<=>CH+H2                          3.000E+13     .000        .00
H+CH3(+M)<=>CH4(+M)                       13.90E+15    -.534     536.00
     LOW  /  2.620E+33   -4.760   2440.00/
     TROE/   .7830   74.00  2941.00  6964.00 /
H2/2.00/ H2O/6.00/ CH4/3.00/ CO/1.50/ CO2/2.00/ C2H6/3.00/ AR/ .70/
H+CH4<=>CH3+H2                            6.600E+08    1.620   10840.00
```

```
H+HCO(+M)<=>CH2O(+M)                      1.090E+12     .480    -260.00
     LOW  /  2.470E+24   -2.570    425.00/
     TROE/   .7824  271.00  2755.00  6570.00 /
H2/2.00/ H2O/6.00/ CH4/2.00/ CO/1.50/ CO2/2.00/ C2H6/3.00/ AR/ .70/
H+HCO<=>H2+CO                             7.340E+13     .000        .00
H+CH2O(+M)<=>CH2OH(+M)                    5.400E+11     .454    3600.00
     LOW  /  1.270E+32   -4.820   6530.00/
     TROE/   .7187  103.00  1291.00  4160.00 /
H2/2.00/ H2O/6.00/ CH4/2.00/ CO/1.50/ CO2/2.00/ C2H6/3.00/
H+CH2O(+M)<=>CH3O(+M)                     5.400E+11     .454    2600.00
     LOW  /  2.200E+30   -4.800   5560.00/
     TROE/   .7580   94.00  1555.00  4200.00 /
H2/2.00/ H2O/6.00/ CH4/2.00/ CO/1.50/ CO2/2.00/ C2H6/3.00/
H+CH2O<=>HCO+H2                           5.740E+07    1.900    2742.00
H+CH2OH(+M)<=>CH3OH(+M)                   1.055E+12     .500      86.00
     LOW  /  4.360E+31   -4.650   5080.00/
     TROE/   .600  100.00  90000.0  10000.0 /
H2/2.00/ H2O/6.00/ CH4/2.00/ CO/1.50/ CO2/2.00/ C2H6/3.00/
H+CH2OH<=>H2+CH2O                         2.000E+13     .000        .00
H+CH2OH<=>OH+CH3                          1.650E+11     .650    -284.00
H+CH2OH<=>CH2(S)+H2O                      3.280E+13    -.090     610.00
H+CH3O(+M)<=>CH3OH(+M)                    2.430E+12     .515      50.00
     LOW  /  4.660E+41   -7.440   14080.0/
     TROE/   .700  100.00  90000.0 10000.00 /
H2/2.00/ H2O/6.00/ CH4/2.00/ CO/1.50/ CO2/2.00/ C2H6/3.00/
H+CH3O<=>H+CH2OH                          4.150E+07    1.630    1924.00
H+CH3O<=>H2+CH2O                          2.000E+13     .000        .00
H+CH3O<=>OH+CH3                           1.500E+12     .500    -110.00
H+CH3O<=>CH2(S)+H2O                       2.620E+14    -.230    1070.00
H+CH3OH<=>CH2OH+H2                        1.700E+07    2.100    4870.00
H+CH3OH<=>CH3O+H2                         4.200E+06    2.100    4870.00
H+C2H(+M)<=>C2H2(+M)                      1.000E+17   -1.000        .00
     LOW  /  3.750E+33   -4.800   1900.00/
     TROE/   .6464  132.00  1315.00  5566.00 /
H2/2.00/ H2O/6.00/ CH4/2.00/ CO/1.50/ CO2/2.00/ C2H6/3.00/ AR/ .70/
H+C2H2(+M)<=>C2H3(+M)                     5.600E+12     .000    2400.00
     LOW  /  3.800E+40   -7.270   7220.00/
     TROE/   .7507   98.50  1302.00  4167.00 /
H2/2.00/ H2O/6.00/ CH4/2.00/ CO/1.50/ CO2/2.00/ C2H6/3.00/ AR/ .70/
H+C2H3(+M)<=>C2H4(+M)                     6.080E+12     .270     280.00
     LOW  /  1.400E+30   -3.860   3320.00/
     TROE/   .7820  207.50  2663.00  6095.00 /
H2/2.00/ H2O/6.00/ CH4/2.00/ CO/1.50/ CO2/2.00/ C2H6/3.00/ AR/ .70/
H+C2H3<=>H2+C2H2                          3.000E+13     .000        .00
H+C2H4(+M)<=>C2H5(+M)                     0.540E+12     .454    1820.00
     LOW  /  0.600E+42   -7.620   6970.00/
     TROE/   .9753  210.00   984.00  4374.00 /
H2/2.00/ H2O/6.00/ CH4/2.00/ CO/1.50/ CO2/2.00/ C2H6/3.00/ AR/ .70/
H+C2H4<=>C2H3+H2                          1.325E+06    2.530   12240.00
H+C2H5(+M)<=>C2H6(+M)                     5.210E+17    -.990    1580.00
     LOW  /  1.990E+41   -7.080   6685.00/
     TROE/   .8422  125.00  2219.00  6882.00 /
H2/2.00/ H2O/6.00/ CH4/2.00/ CO/1.50/ CO2/2.00/ C2H6/3.00/ AR/ .70/
H+C2H5<=>H2+C2H4                          2.000E+12     .000        .00
H+C2H6<=>C2H5+H2                          1.150E+08    1.900    7530.00
H+HCCO<=>CH2(S)+CO                        1.000E+14     .000        .00
H+CH2CO<=>HCCO+H2                         5.000E+13     .000    8000.00
H+CH2CO<=>CH3+CO                          1.130E+13     .000    3428.00
H+HCCOH<=>H+CH2CO                         1.000E+13     .000        .00
H2+CO(+M)<=>CH2O(+M)                      4.300E+07    1.500   79600.00
     LOW  /  5.070E+27   -3.420  84350.00/
     TROE/   .9320  197.00  1540.00 10300.00 /
H2/2.00/ H2O/6.00/ CH4/2.00/ CO/1.50/ CO2/2.00/ C2H6/3.00/ AR/ .70/
OH+H2<=>H+H2O                             2.160E+08    1.510    3430.00
2OH(+M)<=>H2O2(+M)                        7.400E+13    -.370        .00
     LOW  /  2.300E+18    -.900  -1700.00/
     TROE/   .7346   94.00  1756.00  5182.00 /
H2/2.00/ H2O/6.00/ CH4/2.00/ CO/1.50/ CO2/2.00/ C2H6/3.00/ AR/ .70/
2OH<=>O+H2O                               3.570E+04    2.400   -2110.00
OH+HO2<=>O2+H2O                           1.450E+13     .000    -500.00
 DUPLICATE
```

```
OH+H2O2<=>HO2+H2O                       2.000E+12     .000     427.00
 DUPLICATE
OH+H2O2<=>HO2+H2O                       1.700E+18     .000   29410.00
 DUPLICATE
OH+C<=>H+CO                             5.000E+13     .000        .00
OH+CH<=>H+HCO                           3.000E+13     .000        .00
OH+CH2<=>H+CH2O                         2.000E+13     .000        .00
OH+CH2<=>CH+H2O                         1.130E+07    2.000    3000.00
OH+CH2(S)<=>H+CH2O                      3.000E+13     .000        .00
OH+CH3(+M)<=>CH3OH(+M)                  2.790E+18   -1.430    1330.00
     LOW  /  4.000E+36   -5.920   3140.00/
     TROE/   .4120  195.0  5900.00  6394.00/
H2/2.00/ H2O/6.00/ CH4/2.00/ CO/1.50/ CO2/2.00/ C2H6/3.00/
OH+CH3<=>CH2+H2O                        5.600E+07    1.600    5420.00
OH+CH3<=>CH2(S)+H2O                     6.440E+17   -1.340    1417.00
OH+CH4<=>CH3+H2O                        1.000E+08    1.600    3120.00
OH+CO<=>H+CO2                           4.760E+07    1.228      70.00
OH+HCO<=>H2O+CO                         5.000E+13     .000        .00
OH+CH2O<=>HCO+H2O                       3.430E+09    1.180    -447.00
OH+CH2OH<=>H2O+CH2O                     5.000E+12     .000        .00
OH+CH3O<=>H2O+CH2O                      5.000E+12     .000        .00
OH+CH3OH<=>CH2OH+H2O                    1.440E+06    2.000    -840.00
OH+CH3OH<=>CH3O+H2O                     6.300E+06    2.000    1500.00
OH+C2H<=>H+HCCO                         2.000E+13     .000        .00
OH+C2H2<=>H+CH2CO                       2.180E-04    4.500   -1000.00
OH+C2H2<=>H+HCCOH                       5.040E+05    2.300   13500.00
OH+C2H2<=>C2H+H2O                       3.370E+07    2.000   14000.00
OH+C2H2<=>CH3+CO                        4.830E-04    4.000   -2000.00
OH+C2H3<=>H2O+C2H2                      5.000E+12     .000        .00
OH+C2H4<=>C2H3+H2O                      3.600E+06    2.000    2500.00
OH+C2H6<=>C2H5+H2O                      3.540E+06    2.120     870.00
OH+CH2CO<=>HCCO+H2O                     7.500E+12     .000    2000.00
2HO2<=>O2+H2O2                          1.300E+11     .000   -1630.00
 DUPLICATE
2HO2<=>O2+H2O2                          4.200E+14     .000   12000.00
 DUPLICATE
HO2+CH2<=>OH+CH2O                       2.000E+13     .000        .00
HO2+CH3<=>O2+CH4                        1.000E+12     .000        .00
HO2+CH3<=>OH+CH3O                       3.780E+13     .000        .00
HO2+CO<=>OH+CO2                         1.500E+14     .000   23600.00
HO2+CH2O<=>HCO+H2O2                     5.600E+06    2.000   12000.00
C+O2<=>O+CO                             5.800E+13     .000     576.00
C+CH2<=>H+C2H                           5.000E+13     .000        .00
C+CH3<=>H+C2H2                          5.000E+13     .000        .00
CH+O2<=>O+HCO                           6.710E+13     .000        .00
CH+H2<=>H+CH2                           1.080E+14     .000    3110.00
CH+H2O<=>H+CH2O                         5.710E+12     .000    -755.00
CH+CH2<=>H+C2H2                         4.000E+13     .000        .00
CH+CH3<=>H+C2H3                         3.000E+13     .000        .00
CH+CH4<=>H+C2H4                         6.000E+13     .000        .00
CH+CO(+M)<=>HCCO(+M)                    5.000E+13     .000        .00
     LOW  /  2.690E+28   -3.740   1936.00/
     TROE/   .5757  237.00  1652.00  5069.00 /
H2/2.00/ H2O/6.00/ CH4/2.00/ CO/1.50/ CO2/2.00/ C2H6/3.00/ AR/ .70/
CH+CO2<=>HCO+CO                         1.900E+14     .000   15792.00
CH+CH2O<=>H+CH2CO                       9.460E+13     .000    -515.00
CH+HCCO<=>CO+C2H2                       5.000E+13     .000        .00
CH2+O2=>OH+H+CO                         5.000E+12     .000    1500.00
CH2+H2<=>H+CH3                          5.000E+05    2.000    7230.00
2CH2<=>H2+C2H2                          1.600E+15     .000   11944.00
CH2+CH3<=>H+C2H4                        4.000E+13     .000        .00
CH2+CH4<=>2CH3                          2.460E+06    2.000    8270.00
CH2+CO(+M)<=>CH2CO(+M)                  8.100E+11     .500    4510.00
     LOW  /  2.690E+33   -5.110   7095.00/
     TROE/   .5907  275.00  1226.00  5185.00 /
H2/2.00/ H2O/6.00/ CH4/2.00/ CO/1.50/ CO2/2.00/ C2H6/3.00/ AR/ .70/
CH2+HCCO<=>C2H3+CO                      3.000E+13     .000        .00
CH2(S)+N2<=>CH2+N2                      1.500E+13     .000     600.00
CH2(S)+AR<=>CH2+AR                      9.000E+12     .000     600.00
CH2(S)+O2<=>H+OH+CO                     2.800E+13     .000        .00
CH2(S)+O2<=>CO+H2O                      1.200E+13     .000        .00
```

```
CH2(S)+H2<=>CH3+H                         7.000E+13     .000        .00
CH2(S)+H2O(+M)<=>CH3OH(+M)                4.820E+17   -1.160    1145.00
     LOW  /  1.880E+38   -6.360   5040.00/
     TROE/   .6027  208.00  3922.00  10180.0 /
H2/2.00/ H2O/6.00/ CH4/2.00/ CO/1.50/ CO2/2.00/ C2H6/3.00/
CH2(S)+H2O<=>CH2+H2O                      3.000E+13     .000        .00
CH2(S)+CH3<=>H+C2H4                       1.200E+13     .000    -570.00
CH2(S)+CH4<=>2CH3                         1.600E+13     .000    -570.00
CH2(S)+CO<=>CH2+CO                        9.000E+12     .000        .00
CH2(S)+CO2<=>CH2+CO2                      7.000E+12     .000        .00
CH2(S)+CO2<=>CO+CH2O                      1.400E+13     .000        .00
CH2(S)+C2H6<=>CH3+C2H5                    4.000E+13     .000    -550.00
CH3+O2<=>O+CH3O                           3.560E+13     .000   30480.00
CH3+O2<=>OH+CH2O                          2.310E+12     .000   20315.00
CH3+H2O2<=>HO2+CH4                        2.450E+04    2.470    5180.00
2CH3(+M)<=>C2H6(+M)                       6.770E+16   -1.180     654.00
     LOW  /  3.400E+41   -7.030   2762.00/
     TROE/   .6190  73.20  1180.00  9999.00 /
H2/2.00/ H2O/6.00/ CH4/2.00/ CO/1.50/ CO2/2.00/ C2H6/3.00/ AR/ .70/
2CH3<=>H+C2H5                             6.840E+12     .100   10600.00
CH3+HCO<=>CH4+CO                          2.648E+13     .000        .00
CH3+CH2O<=>HCO+CH4                        3.320E+03    2.810    5860.00
CH3+CH3OH<=>CH2OH+CH4                     3.000E+07    1.500    9940.00
CH3+CH3OH<=>CH3O+CH4                      1.000E+07    1.500    9940.00
CH3+C2H4<=>C2H3+CH4                       2.270E+05    2.000    9200.00
CH3+C2H6<=>C2H5+CH4                       6.140E+06    1.740   10450.00
HCO+H2O<=>H+CO+H2O                        1.500E+18   -1.000   17000.00
HCO+M<=>H+CO+M                            1.870E+17   -1.000   17000.00
H2/2.00/ H2O/ .00/ CH4/2.00/ CO/1.50/ CO2/2.00/ C2H6/3.00/
HCO+O2<=>HO2+CO                           13.45E+12     .000     400.00
CH2OH+O2<=>HO2+CH2O                       1.800E+13     .000     900.00
CH3O+O2<=>HO2+CH2O                        4.280E-13    7.600   -3530.00
C2H+O2<=>HCO+CO                           1.000E+13     .000    -755.00
C2H+H2<=>H+C2H2                           5.680E+10    0.900    1993.00
C2H3+O2<=>HCO+CH2O                        4.580E+16   -1.390    1015.00
C2H4(+M)<=>H2+C2H2(+M)                    8.000E+12     .440   86770.00
     LOW  /  1.580E+51   -9.300  97800.00/
     TROE/   .7345  180.00  1035.00  5417.00 /
H2/2.00/ H2O/6.00/ CH4/2.00/ CO/1.50/ CO2/2.00/ C2H6/3.00/ AR/ .70/
C2H5+O2<=>HO2+C2H4                        8.400E+11     .000    3875.00
HCCO+O2<=>OH+2CO                          3.200E+12     .000     854.00
2HCCO<=>2CO+C2H2                          1.000E+13     .000        .00
N+NO<=>N2+O                               2.700E+13     .000     355.00
N+O2<=>NO+O                               9.000E+09    1.000    6500.00
N+OH<=>NO+H                               3.360E+13     .000     385.00
N2O+O<=>N2+O2                             1.400E+12     .000   10810.00
N2O+O<=>2NO                               2.900E+13     .000   23150.00
N2O+H<=>N2+OH                             3.870E+14     .000   18880.00
N2O+OH<=>N2+HO2                           2.000E+12     .000   21060.00
N2O(+M)<=>N2+O(+M)                        7.910E+10     .000   56020.00
     LOW  /  6.370E+14     .000  56640.00/
H2/2.00/ H2O/6.00/ CH4/2.00/ CO/1.50/ CO2/2.00/ C2H6/3.00/ AR/ .625/
HO2+NO<=>NO2+OH                           2.110E+12     .000    -480.00
NO+O+M<=>NO2+M                            1.060E+20   -1.410        .00
H2/2.00/ H2O/6.00/ CH4/2.00/ CO/1.50/ CO2/2.00/ C2H6/3.00/ AR/ .70/
NO2+O<=>NO+O2                             3.900E+12     .000    -240.00
NO2+H<=>NO+OH                             1.320E+14     .000     360.00
NH+O<=>NO+H                               4.000E+13     .000        .00
NH+H<=>N+H2                               3.200E+13     .000     330.00
NH+OH<=>HNO+H                             2.000E+13     .000        .00
NH+OH<=>N+H2O                             2.000E+09    1.200        .00
NH+O2<=>HNO+O                             4.610E+05    2.000    6500.00
NH+O2<=>NO+OH                             1.280E+06    1.500     100.00
NH+N<=>N2+H                               1.500E+13     .000        .00
NH+H2O<=>HNO+H2                           2.000E+13     .000   13850.00
NH+NO<=>N2+OH                             2.160E+13    -.230        .00
NH+NO<=>N2O+H                             3.650E+14    -.450        .00
NH2+O<=>OH+NH                             3.000E+12     .000        .00
NH2+O<=>H+HNO                             3.900E+13     .000        .00
NH2+H<=>NH+H2                             4.000E+13     .000    3650.00
NH2+OH<=>NH+H2O                           9.000E+07    1.500    -460.00
```

```
NNH<=>N2+H                                3.300E+08     .000        .00
NNH+M<=>N2+H+M                            1.300E+14    -.110    4980.00
H2/2.00/ H2O/6.00/ CH4/2.00/ CO/1.50/ CO2/2.00/ C2H6/3.00/ AR/ .70/
NNH+O2<=>HO2+N2                           5.000E+12     .000        .00
NNH+O<=>OH+N2                             2.500E+13     .000        .00
NNH+O<=>NH+NO                             7.000E+13     .000        .00
NNH+H<=>H2+N2                             5.000E+13     .000        .00
NNH+OH<=>H2O+N2                           2.000E+13     .000        .00
NNH+CH3<=>CH4+N2                          2.500E+13     .000        .00
H+NO+M<=>HNO+M                            4.480E+19   -1.320     740.00
H2/2.00/ H2O/6.00/ CH4/2.00/ CO/1.50/ CO2/2.00/ C2H6/3.00/ AR/ .70/
HNO+O<=>NO+OH                             2.500E+13     .000        .00
HNO+H<=>H2+NO                             9.000E+11     .720     660.00
HNO+OH<=>NO+H2O                           1.300E+07    1.900    -950.00
HNO+O2<=>HO2+NO                           1.000E+13     .000   13000.00
CN+O<=>CO+N                               7.700E+13     .000        .00
CN+OH<=>NCO+H                             4.000E+13     .000        .00
CN+H2O<=>HCN+OH                           8.000E+12     .000    7460.00
CN+O2<=>NCO+O                             6.140E+12     .000    -440.00
CN+H2<=>HCN+H                             2.950E+05    2.450    2240.00
NCO+O<=>NO+CO                             2.350E+13     .000        .00
NCO+H<=>NH+CO                             5.400E+13     .000        .00
NCO+OH<=>NO+H+CO                          0.250E+13     .000        .00
NCO+N<=>N2+CO                             2.000E+13     .000        .00
NCO+O2<=>NO+CO2                           2.000E+12     .000   20000.00
NCO+M<=>N+CO+M                            3.100E+14     .000   54050.00
H2/2.00/ H2O/6.00/ CH4/2.00/ CO/1.50/ CO2/2.00/ C2H6/3.00/ AR/ .70/
NCO+NO<=>N2O+CO                           1.900E+17   -1.520     740.00
NCO+NO<=>N2+CO2                           3.800E+18   -2.000     800.00
HCN+M<=>H+CN+M                            1.040E+29   -3.300  126600.00
H2/2.00/ H2O/6.00/ CH4/2.00/ CO/1.50/ CO2/2.00/ C2H6/3.00/ AR/ .70/
HCN+O<=>NCO+H                             2.030E+04    2.640    4980.00
HCN+O<=>NH+CO                             5.070E+03    2.640    4980.00
HCN+O<=>CN+OH                             3.910E+09    1.580   26600.00
HCN+OH<=>HOCN+H                           1.100E+06    2.030   13370.00
HCN+OH<=>HNCO+H                           4.400E+03    2.260    6400.00
HCN+OH<=>NH2+CO                           1.600E+02    2.560    9000.00
H+HCN(+M)<=>H2CN(+M)                      3.300E+13     .000        .00
      LOW /  1.400E+26   -3.400    1900.00/
H2/2.00/ H2O/6.00/ CH4/2.00/ CO/1.50/ CO2/2.00/ C2H6/3.00/ AR/ .70/
H2CN+N<=>N2+CH2                           6.000E+13     .000     400.00
C+N2<=>CN+N                               6.300E+13     .000   46020.00
CH+N2<=>HCN+N                             3.120E+09    0.880   20130.00
CH+N2(+M)<=>HCNN(+M)                      3.100E+12     .150        .00
     LOW  /  1.300E+25   -3.160    740.00/
     TROE/   .6670  235.00  2117.00  4536.00 /
H2/2.00/ H2O/6.00/ CH4/2.00/ CO/1.50/ CO2/2.00/ C2H6/3.00/ AR/ 1.0/
CH2+N2<=>HCN+NH                           1.000E+13     .000   74000.00
CH2(S)+N2<=>NH+HCN                        1.000E+11     .000   65000.00
C+NO<=>CN+O                               1.900E+13     .000        .00
C+NO<=>CO+N                               2.900E+13     .000        .00
CH+NO<=>HCN+O                             4.100E+13     .000        .00
CH+NO<=>H+NCO                             1.620E+13     .000        .00
CH+NO<=>N+HCO                             2.460E+13     .000        .00
CH2+NO<=>H+HNCO                           3.100E+17   -1.380    1270.00
CH2+NO<=>OH+HCN                           2.900E+14    -.690     760.00
CH2+NO<=>H+HCNO                           3.800E+13    -.360     580.00
CH2(S)+NO<=>H+HNCO                        3.100E+17   -1.380    1270.00
CH2(S)+NO<=>OH+HCN                        2.900E+14    -.690     760.00
CH2(S)+NO<=>H+HCNO                        3.800E+13    -.360     580.00
CH3+NO<=>HCN+H2O                          9.600E+13     .000   28800.00
CH3+NO<=>H2CN+OH                          1.000E+12     .000   21750.00
HCNN+O<=>CO+H+N2                          2.200E+13     .000        .00
HCNN+O<=>HCN+NO                           2.000E+12     .000        .00
HCNN+O2<=>O+HCO+N2                        1.200E+13     .000        .00
HCNN+OH<=>H+HCO+N2                        1.200E+13     .000        .00
HCNN+H<=>CH2+N2                           1.000E+14     .000        .00
HNCO+O<=>NH+CO2                           9.800E+07    1.410    8500.00
HNCO+O<=>HNO+CO                           1.500E+08    1.570   44000.00
HNCO+O<=>NCO+OH                           2.200E+06    2.110   11400.00
HNCO+H<=>NH2+CO                           2.250E+07    1.700    3800.00
```

```
HNCO+H<=>H2+NCO                           1.050E+05    2.500   13300.00
HNCO+OH<=>NCO+H2O                         3.300E+07    1.500    3600.00
HNCO+OH<=>NH2+CO2                         3.300E+06    1.500    3600.00
HNCO+M<=>NH+CO+M                          1.180E+16     .000   84720.00
H2/2.00/ H2O/6.00/ CH4/2.00/ CO/1.50/ CO2/2.00/ C2H6/3.00/ AR/ .70/
HCNO+H<=>H+HNCO                           2.100E+15    -.690    2850.00
HCNO+H<=>OH+HCN                           2.700E+11     .180    2120.00
HCNO+H<=>NH2+CO                           1.700E+14    -.750    2890.00
HOCN+H<=>H+HNCO                           2.000E+07    2.000    2000.00
HCCO+NO<=>HCNO+CO                         0.900E+13     .000        .00
CH3+N<=>H2CN+H                            6.100E+14    -.310     290.00
CH3+N<=>HCN+H2                            3.700E+12     .150     -90.00
NH3+H<=>NH2+H2                            5.400E+05    2.400    9915.00
NH3+OH<=>NH2+H2O                          5.000E+07    1.600     955.00
NH3+O<=>NH2+OH                            9.400E+06    1.940    6460.00
NH+CO2<=>HNO+CO                           1.000E+13     .000   14350.00
CN+NO2<=>NCO+NO                           6.160E+15   -0.752     345.00
NCO+NO2<=>N2O+CO2                         3.250E+12     .000    -705.00
N+CO2<=>NO+CO                             3.000E+12     .000   11300.00
O+CH3=>H+H2+CO                            3.370E+13     .000        .00
O+C2H4<=>H+CH2CHO                         6.700E+06    1.830     220.00
O+C2H5<=>H+CH3CHO                         1.096E+14     .000        .00
OH+HO2<=>O2+H2O                           0.500E+16     .000   17330.00
  DUPLICATE
OH+CH3=>H2+CH2O                           8.000E+09     .500   -1755.00
CH+H2(+M)<=>CH3(+M)                       1.970E+12     .430    -370.00
   LOW/ 4.820E+25  -2.80  590.0 /
   TROE/ .578  122.0  2535.0  9365.0 /
H2/2.00/ H2O/6.00/ CH4/2.00/ CO/1.50/ CO2/2.00/ C2H6/3.00/ AR/ .70/
CH2+O2=>2H+CO2                            5.800E+12     .000    1500.00
CH2+O2<=>O+CH2O                           2.400E+12     .000    1500.00
CH2+CH2=>2H+C2H2                          2.000E+14     .000   10989.00
CH2(S)+H2O=>H2+CH2O                       6.820E+10     .250    -935.00
C2H3+O2<=>O+CH2CHO                        3.030E+11     .290      11.00
C2H3+O2<=>HO2+C2H2                        1.337E+06    1.610    -384.00
O+CH3CHO<=>OH+CH2CHO                      2.920E+12     .000    1808.00
O+CH3CHO=>OH+CH3+CO                       2.920E+12     .000    1808.00
O2+CH3CHO=>HO2+CH3+CO                     3.010E+13     .000   39150.00
H+CH3CHO<=>CH2CHO+H2                      2.050E+09    1.160    2405.00
H+CH3CHO=>CH3+H2+CO                       2.050E+09    1.160    2405.00
OH+CH3CHO=>CH3+H2O+CO                     2.343E+10    0.730   -1113.00
HO2+CH3CHO=>CH3+H2O2+CO                   3.010E+12     .000   11923.00
CH3+CH3CHO=>CH3+CH4+CO                    2.720E+06    1.770    5920.00
H+CH2CO(+M)<=>CH2CHO(+M)                  4.865E+11    0.422   -1755.00
    LOW/ 1.012E+42  -7.63  3854.0/
    TROE/ 0.465  201.0  1773.0  5333.0 /
H2/2.00/ H2O/6.00/ CH4/2.00/ CO/1.50/ CO2/2.00/ C2H6/3.00/ AR/ .70/
O+CH2CHO=>H+CH2+CO2                       1.500E+14     .000       .00
O2+CH2CHO=>OH+CO+CH2O                     1.810E+10     .000       .00
O2+CH2CHO=>OH+2HCO                        2.350E+10     .000       .00
H+CH2CHO<=>CH3+HCO                        2.200E+13     .000       .00
H+CH2CHO<=>CH2CO+H2                       1.100E+13     .000       .00
OH+CH2CHO<=>H2O+CH2CO                     1.200E+13     .000       .00
OH+CH2CHO<=>HCO+CH2OH                     3.010E+13     .000       .00
CH3+C2H5(+M)<=>C3H8(+M)                   .9430E+13     .000       .00
     LOW/ 2.710E+74  -16.82  13065.0 /
     TROE/ .1527  291.0  2742.0  7748.0 /
H2/2.00/ H2O/6.00/ CH4/2.00/ CO/1.50/ CO2/2.00/ C2H6/3.00/ AR/ .70/
O+C3H8<=>OH+C3H7                          1.930E+05    2.680   3716.00
H+C3H8<=>C3H7+H2                          1.320E+06    2.540   6756.00
OH+C3H8<=>C3H7+H2O                        3.160E+07    1.800    934.00
C3H7+H2O2<=>HO2+C3H8                      3.780E+02    2.720   1500.00
CH3+C3H8<=>C3H7+CH4                       0.903E+00    3.650   7154.00
CH3+C2H4(+M)<=>C3H7(+M)                   2.550E+06    1.600   5700.00
      LOW/ 3.00E+63  -14.6  18170./
      TROE/ .1894  277.0  8748.0  7891.0 /
H2/2.00/ H2O/6.00/ CH4/2.00/ CO/1.50/ CO2/2.00/ C2H6/3.00/ AR/ .70/
O+C3H7<=>C2H5+CH2O                        9.640E+13     .000       .00
H+C3H7(+M)<=>C3H8(+M)                     3.613E+13     .000       .00
      LOW/ 4.420E+61  -13.545  11357.0/
      TROE/ .315  369.0  3285.0  6667.0 /
```

```
H2/2.00/ H2O/6.00/ CH4/2.00/ CO/1.50/ CO2/2.00/ C2H6/3.00/ AR/ .70/
H+C3H7<=>CH3+C2H5                         4.060E+06    2.190    890.00
OH+C3H7<=>C2H5+CH2OH                      2.410E+13     .000       .00
HO2+C3H7<=>O2+C3H8                        2.550E+10    0.255   -943.00
HO2+C3H7=>OH+C2H5+CH2O                    2.410E+13     .000       .00
CH3+C3H7<=>2C2H5                          1.927E+13   -0.320       .00
END
```